PENSOFT
SENCKENBERG world of biodiversity
Leibniz Association

Phylogenetic analysis of rove beetle subfamily Staphylininae (Coleoptera: Staphylinidae) based on the morphology of preimaginal stages, with description of larva and pupa of *Algon sphaericollis*

Chong Li[1], Liang Tang[1]

1 *College of Science, Shanghai Normal University, 100 Guilin Road, 1st Educational Building 323 Room, Shanghai, 200234 P. R. China*

https://zoobank.org/7EB8B9E7-8E72-4E5A-904F-824E7E881CF1

Corresponding author: Liang Tang (staphylinidae@shnu.edu.cn)

Received 15 May 2024
Accepted 29 June 2024
Published 6 December 2024

Academic Editors Martin Fikácek, Klaus-Dieter Klass

Citation: Li C, Tang L (2024) Phylogenetic analysis of rove beetle subfamily Staphylininae (Coleoptera: Staphylinidae) based on the morphology of preimaginal stages, with description of larva and pupa of *Algon sphaericollis*. Arthropod Systematics & Phylogeny 82: 629–657. https://doi.org/10.3897/asp.82.e106391

Abstract

Staphylininae, a highly diverse subfamily of rove beetles (Coleoptera: Staphylinidae), has been the subject of numerous phylogenetic studies primarily based on molecular genetics and adult morphology. This work represents an initiation of phylogenetic studies using complete immature morphology, encompassing eggs, larvae and pupae, for 27 genera of Staphylininae and two outgroups. Our findings indicate that the combination of data from all three immature stages is more phylogenetically informative than the larval data alone. The resulting maximum parsimony tree partially aligns with previous research, although certain tribal-level issues remain unresolved. Through morphological comparisons, we revealed the morphological diversity of protibia, paratergites and parasternites of abdominal segment I as examples of parallel and mosaic evolution within Staphylininae larvae. We conducted detailed character analyses to provide explanations for these phenomena. Furthermore, this study provides the first morphological data for several species of Staphylinini. Notably, we present a comprehensive study of the morphology of immature stages of *Algon sphaericollis* Schillhammer, 2006, the first species of the recently established subtribe Algonina with known larva. Additionally, we provide the larval morphology data for six other species: *Eucibdelus* sp., *Platydracus pseudopaganus pseudopatricius* (Müller, 1926), *Platydracus marmorellus* (Fauvel, 1895), *Saniderus cooteri* Rougemont, 2015, *Saniderus* sp., and *Philonthus spinipes* Sharp, 1874.

Key words

Algonina, immature stages, larva, morphology, phylogeny, Staphylininae

1. Introduction

The rove beetles (Staphylinidae) constitute the largest family in the entire animal kingdom, and the Staphylininae is one of its most diverse subfamilies, even after a recent revision moved some of its members to other subfamilies (Żyła and Solodovnikov 2019). Over the past decade, a series of systematic studies have attempted to unveil the evolutionary history of this subfamily through phylogenetic analyses using adult morphological data (Solodovnikov and Schomann 2009; Brunke and Solodovnikov, 2013), molecular data (Chatziman-

olis et al. 2010; Chani-Posse et al. 2018), and fossils (Solodovnikov et al. 2013; Brunk et al. 2017). These studies revealed that the ancestors of Staphylininae originated in the Late Jurassic. The drifting of land masses subsequently led to the division of Staphylininae into the Southern and Northern hemisphere clades, with the former including the basal and stem group lineages, and the latter forming the crown group (Brunke et al. 2016). These phylogenetic conclusions also led to revisions in taxonomy, notably within the diverse Quediini and Staphylinini. Some of the former Quediini members were reclassified into the early-branching groups such as Amblyopinini, Acylophorini, Tanygnathinini, Cyrtoquediini, with the northern temperate members classified as the true Quediini (Solodovnikov and Schomann 2009). The species-diverse tribe Staphylinini also belongs to the Northern hemisphere clade, originally called 'Staphylinini propria' by Chatzimanolis et al. (2010). This tribe comprises of four subtribes (Philonthina, Staphylinina, Xanthopygina, and Anisolinina), and genera classified as incertae sedis. The first three subtribes have been systematically studied recently (Philonthina by Chani-Posse et al. 2018; Staphylinina by Brunke and Smetana 2019; Xanthopygina by Chatzimanolis and Brunke 2019), while Anisolinina is still not clearly defined. Two other recently established subtribes, Algonina and Philothalpina, are relatively small in number of species and are restricted to the Oriental and Neotropical regions, respectively. Algonina is a relatively young but historically complex subtribe, with only 92 recorded species (Li and Tang 2023). The genus *Algon* was initially classified within Xanthopygina due to its adult morphology. However, after phylogenetic studies based on molecular data, it was first reclassified under 'Staphylinini incertae sedis' by Chatzimanolis (2014), and later placed into the new subtribe Algonina by Chani-Posse et al. (2018), together with *Barypalpus* Cameron, 1932. Philothalpina has been also established around that time (Chani-Posse et al. 2018). More recently, *Rientis* Sharp, 1874 was included in Algonina by Żyła and Solodovnikov (2019), and Algonina was recognized as one of the six subtribes within the revised Staphylinini. While these phylogenetic analyses consistently provided high topological congruence at and above the tribe level, relationships between subtribes remained inconclusive or inconsistent among studies using different datasets and phylogenetic methods (Chani-Posse et al. 2018; Żyła and Solodovnikov 2019; Tihelka et al. 2020).

Despite the adult stage represents only a quarter of the morphology expressed during the beetle's life cycle, phylogenetic studies of Staphylininae rely heavily on homoplastic adult morphology, since the research on the immature stages is relatively scarce. Among rove beetles, Staphylininae is the subfamily with the largest number of species with known larval stages. Yet, fewer than 50 out of c. 380 staphylinine genera have documented larval stages (Pototskaya 1967; Pietrykowska-Tudruj et al. 2014; Staniec and Pietrykowska-Tudruj 2019). Even in the species-rich Staphylinini, the larval data is primarily limited to Philonthina and Staphylinina. Rearing larvae from egg to adult involves significant laboratory work, and the identification of larvae collected directly from the field is often not possible. Despite all these difficulties, several studies have provided valuable insights to immature morphology. Notably, studies on Staphylininae based on the combination of adult and larval characters (Solodovnikov and Newton, 2005), larval morphology (Pietrykowska-Tudruj et al. 2012), and pupal morphology (Staniec and Pietrykowska-Tudruj, 2019) has resolved certain species with classification controversies, demonstrating that preimaginal characters can be a useful addition to phylogenetic analyses.

This study aims at exploring the immature stages of key members of the Staphylinini, in order to provide data on additional taxa and conduct phylogenetic analysis combining all known data on immature Staphylininae. We also want to test the significance of non-adult characters for phylogenetic reconstruction and understand their evolutionary processes. First time even we include egg characters, since eggs of Staphylinini are morphologically diverse, as previous studies by Hinton (1981) and Staniec and Pietrykowska-Tudruj (2007) have documented. We conducted laboratory rearings of immature stages of five genera of Staphylinini, providing the first data for *Algon* Sharp, 1874, *Saniderus* Fauvel, 1895, and *Eucibdelus* Kraatz, 1859. As the special part of this study, we conducted an in-depth morphological study on *Algon sphaericollis* Schillhammer, 2006 (Fig. 1A, B), i.e. the first member of Algonina with known immature stages, in order to gather complete data on its biology and life cycle.

2. Material and methods

2.1. Rearings and specimen examination

The preimaginal stages of the following species were studied for the first time (the origin of specimens used for rearing is indicated). They were obtained in laboratory by rearing adults collected from field, except for *Platydracus p. pseudopatricius*, in which the larvae were collected in the field and reared to adults.

Algon sphaericollis Schillhammer, 2006: collected from November 2021 to October 2022 by sifting the forest leaf litter in Minhang, Shanghai, China (31°1′11″N 121°28′1″E).

Philonthus spinipes Sharp, 1874: collected from November 2021 to October 2022 by sifting the forest leaf litter in Minhang, Shanghai, China (31°1′11″N 121°28′1″E).

Platydracus pseudopaganus pseudopatricius (M**ü**ller, 1926): collected on June 3, 2021 by sifting in the bamboo forest of Sheshan Mountain, Shanghai, China (31°6′12″N 121°12′3″E).

Platydracus marmorellus (Fauvel, 1895): collected on August 10, 2021 from Qingchengshan Mt., Sichuan, China (30°54′38″N 103°34′26″E).

Saniderus cooteri Rougemont, 2015: collected on May 1, 2021 in Ruyuan, Shaoguan County, Guangdong, China (24°55′56″N 113°1′41″E).

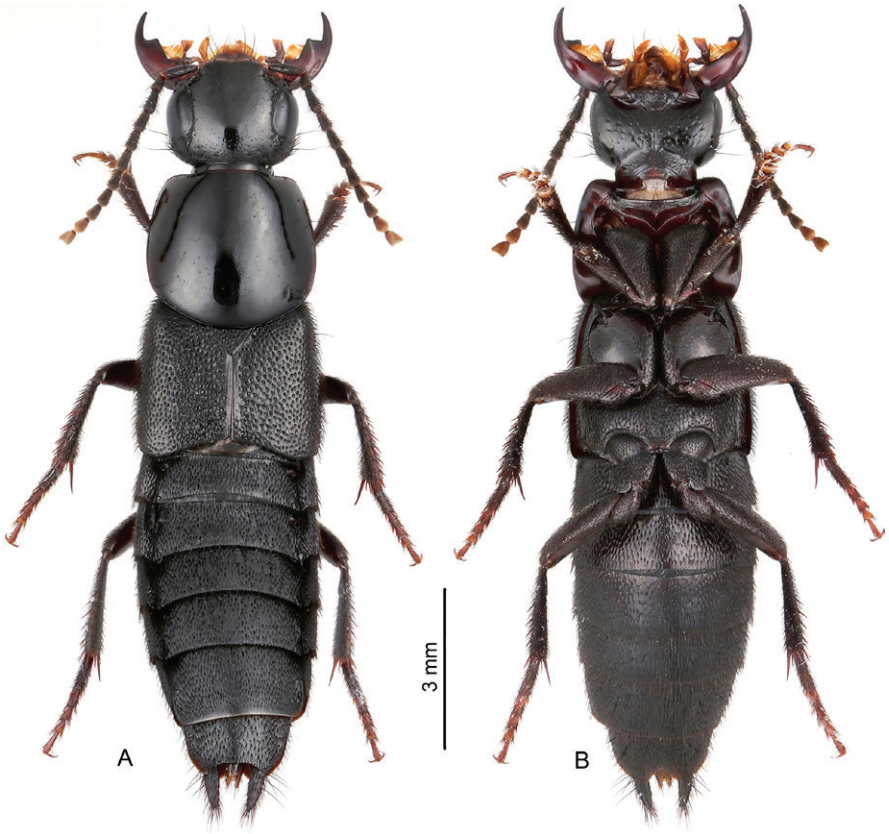

Figure 1. Male adult habitus of *Algon sphaericollis* Schillhammer, 2006.

Eucibdelus sp.: collected on May 1, 2021 in Ruyuan, Shaoguan County, Guangdong, China (24°55′56″N 113°1′41″E).

Saniderus sp.: collected on August 3, 2021 by sifting in the bamboo forest near the expressway of Xiling snow mountain of Sichuan, China (30°37′39″N 103°23′8″E).

Field collected adults or larvae of each species were placed in a plastic container filled with humid soil and covered with moist tissue. When the daily temperature reached 20°C, females and males were paired in boxes for mating. After oviposition, the eggs were placed separately in plastic boxes filled with moist tissue (laboratory temperature 22 ± 2°C) for daily observation. Hatched larvae were kept in a plastic box covered with moist tissue. *Blatta lateralis* (Walker, 1868) were supplied as food for both adults and larvae. Development time at each stage was recorded. When larvae of successive instars and prepupae were obtained, several individuals that reached those stages were killed and preserved.

For morphological descriptions, a few larvae of each instar were killed with boiling water and immediately after killing placed in a groove of an acrylic plate filled with 75% ethanol and covered with a cover glass. After removing air bubbles, they were photographed using Canon macro photo lens MP-E 65 mm attached to a Canon EOS7D camera; photographs were stacked with Zerene Stacker.

For detailed morphological studies, several larvae of each instar were decapitated, macerated in boiling 10% KOH, rinsed in distilled water, dried by ethanol gradient dehydration, and mounted in Euparal (Chroma Gesellschaft Schmidt, Koengen, Germany) on plastic slides. Photos of taxonomic characters were taken with a Canon G9 camera attached to an Olympus SZX 16 stereoscope. Some of the features used for morphological research were drawn for clearer outlines. To obtain the microscopic structure of eggs and larva, samples were dried by ethanol gradient dehydration, and scanned by HITACHI UHR FE-SEM SU 8000 scanning electron microscope. The material used for each species is listed in Table 1. Voucher specimens are deposited in the Department of Biology, Shanghai Normal University, P. R. China (SHNU).

The life cycle of *Algon sphaericollis* in Shanghai was studied from November 2020 to October 2022 by rearing in the laboratory with simultaneous observation in the field. Adults were searched every ten days in the field by turning over rocks and sifting leaves. Habitat preferences were investigated in the field.

Compared with adults, the morphological terminology of immature stages of Staphylinidae is still not unified. We follow Schmidt (1996) and Staniec et al. (2009) for the terminology of the structures of egg, larva and pupa, functional organs, sclerites and setae, and Solodovnikov and Newton (2005) for the terminology of the larval thorax. The terminology of chaetotaxy follows Ashe and Watrous (1984), Solodovnikov and Newton (2005) and Pietrykowska-Tudruj et al. (2014). Only the detailed morphological study of *A. sphaericollis* is presented in this paper. The second instar larvae (L_2) of *A. sphaericollis* are very similar to the L_3 larvae and are hence not described.

Table 1. Material used for morphological and biological study of each species.

Taxon	Adults	Eggs	L_1	L_2	L_3	Prepupa	Pupae
Algon sphaericollis Schillhammer, 2006	18	10	7	2	5	1	3
Eucibdelus sp.	3	9	5	3	—	—	—
Platydracus pseudopaganus pseudopatricius (Müller, 1926)	—	—	1	3	10	—	3
Platydracus marmorellus (Fauvel, 1895)	3	14	7	5	10	—	3
Saniderus cooteri Rougemont, 2015	1	1	—	1	—	—	—
Saniderus sp.	5	22	6	4	8	—	2
Philonthus spinipes Sharp, 1874	1	1	3	2	5	—	3

2.2. Phylogenetic analysis

For the phylogenetic analysis, we combined the species we reared by ourselves, and those described in the literature. Considering that the larval studies of *Ontholestes murinus* by Paulian (1941) and Potoskaya (1967) lack a lot of important morphological data, the morphology of this species was coded based on the examination of the third instar larvae deposited in the Zoological Museum of the University of Copenhagen, Denmark by Qing-Hao Zhao. The microstructure of the egg of *Philonthus spinipes* was examined with the help of Mateusz Sapieja (Museum of Natural History, University of Wroctaw, Poland). The following 71 characters were coded for 40 terminal taxa:

1. Egg, shape: (0) Broadly oval, surface without any distinct structures; (1) with longitudinal ridges; (2) with crescent-shaped contact disc anteriorly; (3) with transverse ridge; (4) with numerous pointed projections.
2. Egg, aeropyles: (0) distinct; (1) absent or invisable.
3. Egg, aeropyles, arrangment: (0) uniformly scattered; (1) longitudinally arranged in several rows; (2) irregularly scattered (3) densely formed band.
4. Egg, aeropyle band, shape: (0) equatorial band; (1) wave-like band.
5. Egg, wave-like aeropyle band: (0) divided; (1) undivided.
6. Egg, transverse ridge: (0) extending over the whole length of equator, forming a closed ring; (1) extending about one third length of equator.
7. Head capsule, length/wide (without neck): (0) distinctly longer than wide; (1) almost as long as wide.
8. Head capsule, ventral ecdysial line: (0) Y-shaped; (1) anterior arms atrophied.
9. Head capsule, apotome: (0) with stalk; (1) without stalk.
10. Head capsule, tentorial pits: (0) placed anteriorly; (1) placed centrally; (2) placed posteriorly.
11. Head capsule, frayed or club-shaped setae: (0) abscent; (1) present.
12. Head, epicranial gland; (0) present; (1) absent.
13. Head, position of macro epicranial dorsal setae: (0) the connection between the two setae divides the medial ecdysial line (without neck) into a shorter front half and a longer back half, with a ratio of the two less than 0.5 (Fig. 15M); (1) the connection between two setae divides the ecdysial line into two segments of almost equal length, with the ratio of the front half to the back half between 0.5 and 1 (Fig. 15L). (2) the connection between two setae almost reach to the bottom of nasale.
14. Nasale, number of teeth: (0) 9; (1) 7; (2) 11
15. Nasale, median tooth: (0) distinct; (1) barely visible.
16. Antennae, segment IV: (0) longer than sensory appenda ge; (1) shorter than sensory appendage.
17. Antennae, sensory appendage located: (0) inner laterally; (1) ventrally; (2) outter laterally.
18. Antenna, sclerotized band of main sensory appendage: (0) present; (1) absent.
19. Ligula: (0) sclerotised; (1) unsclerotised.
20. Maxillae, setae on inner margin of segment II of maxillary palp, position: (0) apical, within top 1/3; (1) middle; (2) lower middle, about 1/3 of the base; (3) lower, less than 1/4 of the base.
21. Maxillae, digitiform sensory appendage location: (0) at base of segment III; (1) anteriorly, closer to apex.
22. Maxillae, mala: (0) as long as or longer than segment I of maxillary palp; (1) shorter than segment I of maxillary palp but longer than 1/3 the maxillary palp segment I; (2) shorter than 1/3 the maxillary palp segment I.
23. Maxillae, mala, apical setae: (0) present; (1) absent.
24. Maxillae, mala, number of apical setae: (0) 1; (1) 2; (2) 3.
25. Maxillae, mala, setae on inner magin: (0) present; (1) absent.
26. Maxillae, mala, setae on outer magin: (0) present; (1) absent.
27. Maxillae, mala, setae near base: (0) present; (1) absent.
28. Maxillary palp and labial palp, last segment: (0) with notch of thinner sclerotization, (1) without notch of thinner sclerotization.
29. Maxillary palp and labial palp: (0) four and three segments, respectively; (1) three and two segments, respectively; (2) three and three segments, respectively.
30. Labial palp, segment I: (0) with pore, (1) without pore.
31. Stemmata (if not atrophied): (0) four pairs; (1) six pairs; (2) one pair; (3) three pairs.
32. Prothorax, spiracal appendage: (0) absent; (1) present.
33. Prothorax, frayed or club-shaped setae: (0) absent; (1) present.

34. Meso- and metathorax, frayed or club-shaped setae: (0) absent; (1) present.
35. Protibia: (0) length/width between 4 and 6, parallel-sided at two thirds of base or slightly dilate at middle; (1) tubby, length/width < 4, dilated anteriorly; (2) very slender, almost as long as femur, length/width > 6, widest near base, gradually tapering toward front; (3) very slender, almost as long as femur, length/width > 6, widest at 1/3 base, then suddenly taper toward front.
36. Protibia, type of setae: (0) scattered big spines, rarely with smaller spines; (1) numerous short setae; (2) densely distributed large spines, with smaller spines scattered among them.
37. Bifurcate setae on protibia: (0) present; (1) absent.
38. Protibia, comb: (0) present; (1) absent.
39. Protibia, rows of comb: (0) single; (1) multipal.
40. Protibia, comb, type of setae: (0) bifurcate; (1) simple.
41. Foreleg, tarsungulus: (0) fused with tibia; (1) not fused with tibia.
42. Foreleg, tarsungulus, number of spine-like setae: (0) 2; (1) 3; (2) 4; (3) 8.
43. Foreleg, tarsungulus, bifurcate setae: (0) present; (1) absent.
44. Foreleg, tarsungulus, spine-like setae on dorsal side: (0) absent; (1) present.
45. Foreleg, tarsungulus, spine-like setae on dorsal side: (0) as long as ventral setae; (1) longer than ventral setae.
46. Foreleg, trochanter, length of spine-like setae on ventral front: (0) at least twice the thickness of trochanter; (1) less than twice the thickness of trochanter.
47. Abdominal paratergites of segment II–VIII: (0) fused as a whole; (1) divided into two parts.
48. Abdominal, paratergites and parasternites of segment I: (0) present; (1) absent.
49. Abdominal, paratergites and parasternites of segment I, shape: (0) similar with segment II-VIII; (1) differed from segment II-VIII.
50. Abdominal, paratergites and parasternites of segment I: (0) paratergites bend toward the parasternites; (1) paratergites in their usual form, parasternites reduced into tiny fragments, with an additional posterior sclerite emerging between them (Fig. 16K); (2) paratergites and parasternites seamlessly merge forming U-shaped lateral sclerites; (3) paratergites and parasternites fused with more distinct boundaries at the smaller parasternites.
51. Abdominal, posterior carina of tergite I: (0) absent; (1) present.
52. Abdominal, tergites, setae on segment II–VIII, (0) only frayed or club-shaped; (1) frayed or club-shaped and simple; (2) only simple.
53. Abdominal, sternites, setae on segment II–VIII, (0) only frayed or club-shaped; (1) frayed or club-shaped and simple; (2) only simple.
54. Urogomphi: (0) longer than pygopod; (1) 0.3–0.8 × as long as pygopod; (2) 0.9–1.1 × as long as pygopod.
55. Urogomphi: (0) 2 segments; (1) not segmented, fusiform; (2) not segmented, whip-like.
56. Urogomphi, segment I, frayed or club-shaped setae: (0) present; (1) absent.
57. Urogomphi, segment I, simple macro setae: (0) present; (1) absent.
58. Urogomphi, segment II, frayed or club-shaped setae: (0) present; (1) absent.
59. Pygopod, shape: (0) short, 1.1–1.8 as long as wide; (1) moderately elongate, 2.1–3.1 as long as wide.
60. Pupae, Setiform projections or spines on body (excluding segment IX): (0) present; (1) absent.
61. Pupae, protuberances on pronotum: (0) present; (1) absent.
62. Pupae, setiform projections on pronotum: (0) present; (1) absent.
63. Pupae, protuberances on mesonotum: (0) present; (1) absent.
64. Pupae, cuticular processes on sides of abdominal segment VII: (0) present; (1) absent.
65. Pupae, cuticular processes on sides of abdominal segment VIII: (0) present; (1) absent.
66. Pupae, type of cuticular processes on sides of abdominal: (0) setiform projections; (1) spines.
67. Pupae, terminal prolongations of segment IX: (0) present; (1) absent.
68. Pupae, apical accessories of terminal prolongations: (0) present; (1) absent.
69. Pupae, shape of apical accessories: (0) straight; (1) curved.
70. Pupae, apex of apical accessories: (0) pointed; (1) rounded.
71. Pupae, first pairs of functional spiracles: (0) in the same longitudinal line as others; (1) protruding laterally much more than others.

Information about the morphology of immature stages of other species used in the analysis (26 genera of Staphylininae representing 7 tribes sensu Żyła and Solodovnikov 2020) is extracted from the literature; members of Platyprosopinae and Xantholininae are added as outgroups (Table 2). A data matrix of 71 morphological characters including eggs, mature larvae (or L_2 when mature larvae were unavailable) and pupae is coded for 40 terminal taxa (File S1). Inapplicable characters are marked by '–' and treated equivalent to missing data (?). The majority of terminal taxa are comprised of a single species, with exceptions of genera which species share the same morpohlogy (e.g., *Saniderus*, *Arrowinus*, and *Erichsonius*) or when morphology data of a species with incomplete information can be completed by the data of other species of the same genus (e.g., the data of *Xanthopygus* were extracted from the data matrix of Solodovnikov (2005) and complemented data provided for *X. cognatus* by Quezada et al. 1969). The data matrix was imported into TNT 1.1. (Goloboff et al. 2008) and analyzed with equally weighted parsimony and traditional search: the memory was set to hold 10000 trees, 1000 replicates with tree bisection-reconnection (TBR) swapping and holding 10 trees per replicate. The results were visualized in WinClada v. 1.00.08.

Table 2. Information of immature data sources for phylogenetic analysis. Classification a subfamily and tribe level follows Żyła and Solodovnikov (2019).

Species	Stage	References
Tribe Staphylinini		
Creophilus maxillosus (Linné, 1758)	egg, L_3, pupa	Voris (1939); Paulian (1941); Pototskaya (1967); Dajoz and Caussanel (1968); Hinton (1981); Staniec and Pietrykowska-Tudruj (2019)
Ocypus fulvipennis Erichson, 1840	egg, L_3, pupa	Staniec et al. (2009)
Ontholestes murinus (Linnaeus, 1758)	egg, L_3, pupa	Pototskaya (1967); Hinton (1981); Staniec (2004)
Ontholestes cingulatus Gravenhorst, 1802	egg, L_3, pupa	Voris (1939); Kasule (1970)
Staphylinus erythropterus Linné, 1758	egg, L_2, pupa	Hinton (1981); Pietrykowska-Tudruj and Staniec (2012)
Platydracus tomentosus (Gravenhorst, 1802)	egg, L_3, pupa	Schmidt (1994a)
Platydracus latebricola (Gravenhorst, 1806)	L_3	Pietrykowska-Tudruj and Staniec (2012)
Emus hirtus (Linnaeus, 1758)	egg, L_3, pupa	Zhao and Solodovnikov (2023)
Abemus chloropterus (Panzer, 1796)	L_3	Boháč (1982)
Hesperus rufipennis (Gravenhorst, 1802)	egg, L_3, pupa	Staniec (2004)
Philonthus punctus (Gravenhorst, 1802)	egg, L_3, pupa	Staniec and Pietrykowska-Tudruj (2006a); Staniec, 2003
Philonthus nigrita (Gravenhorst, 1806)	egg, L_3, pupa	Staniec and Pietrykowska-Tudruj (2008)
Gabrius splendidulus (Gravenhorst, 1802)	egg, L_3, pupa	Kasule (1970); Staniec and Pietrykowska-Tudruj (2007); Pietrykowska-Tudruj et al. (2014); Pietrykowska-Tudruj et al. (2019)
Bisnius nitidulus (Gravenhorst, 1802)	egg, L_3, pupa	Staniec and Pietrykowska-Tudruj (2010); Staniec and Kitowski (2004)
Neobisnius sobrinus (Erichson, 1840)		Schmidt (1994b)
Cafius nauticus Fairmaire, 1849	egg, L_3, pupa	Cai and Tang (2022)
Xanthopygus xanthopygus Nordmann, 1837	L_3 (little data)	Solodovnikov and Newton (2005)
Xanthopygus cognatus Sharp, 1876	egg, L_3, pupa (all contain little data)	Quezada et al. (1969)
Tribe Quediini		
Quedius brevicornis (Thomson, 1860)	egg, L_3, pupa	Staniec (2003); Staniec and Pietrykowska-Tudruj (2007)
Quedius brevis Erichson, 1840	egg, L_3, pupa	Pietrykowska-Tudruj and Staniec (2006); Staniec and Pietrykowska-Tudruj (2007); Pietrykowska-Tudruj et al. (2014)
Quedius microps Gravenhorst, 1847	egg, L_3, pupa	Pietrykowska-Tudruj and Staniec (2006); Staniec and Pietrykowska-Tudruj (2007); Pietrykowska-Tudruj et al. (2014)
Quedius fuliginosus (Gravenhorst, 1802)	L_3, pupa	Pototskaya (1967); Staniec (1999); Pietrykowska-Tudruj et al. (2014)
Tribe Acylophorini		
Acylophorus wagenschieberi Kiesenwetter, 1850	egg, L_3, pupa	Staniec (2005a)
Anaquedius vernix (LeConte, 1878)	L_3	LeSage (1984)
Tribe Tanygnathinini		
Atanygnathus terminalis (Erichson, 1839)	egg, L_3, pupa	Staniec (2005b)
Atanygnathus bicolor Casey, 1915	L_3	Solodovnikov (2005)
Tribe Amblyopinini		
Heterothops nigra Kraatz, 1868	L_3 (little data), pupa	Paulian (1941); Pietrykowska-Tudruj and Staniec (2006b)
Heterothops praevia Erichson, 1839	L_3 (little data)	Paulian (1941)
Natalignathus olgae Solodovnikov, 2005	L_3	Solodovnikov (2005)
Quedius antipodum Sharp, 1886	L_3	Pietrykowska-Tudruj et al. (2012)
Tribe Cyrtoquediini		
Astrapaeus ulmi (Rossi, 1790)	egg, L_3, pupa	Pietrykowska-Tudruj et al. (2014)
Tribe Antimerini		
Antimerus punctipennis Lea, 1906	L_3	Solodovnikov and Newton (2010)
Tribe Erichsonini		
Erichsonius alumnus Frank, 1975	Egg, L_3, pupa	Schmidt (1996)
Erichsonius pusio (Horn, 1884)	Egg, L_3, pupa	Schmidt (1996)
Subfamily Platyprosopinae		
Arrowinus phaenomenalis Bernhauer, 1935	L_3	Solodovnikov and Newton (2005)
Arrowinus peckorum Solodovnikov, 2005	L_3	Solodovnikov and Newton (2005)
Subfamily Xantholininae		
Hypnogyra angularis (Ganglbauer, 1895)	Egg, L_3, pupa	Pietrykowska-Tudruj and Staniec (2006c)

3. Results and disscussion

3.1. Morphology of immature stages of *Algon sphaericollis*

Egg (Fig. 2A, B)**.** Early stage: Length: 1.83–2.00 mm (mean 1.92 mm); width: 1.42–1.48 mm (mean 1.45 mm). Late stage: Length: 1.90–2.25 mm (mean 2.08 mm); width: 1.68–1.88 mm (mean 1.78 mm). Colour white, becoming gray and speckled as it develops. shape oval, expanding laterally along its development; half of its length with narrow transverse ridge forming a closed ring; surface rough, aeropyles invisible, with irregular granular protuberance (Fig. 2B).

Mature larva (L_3) (Fig. 2D–F)**.** Body length (from anterior margin of nasale to end of pygopod): 15.96–17.70 mm (mean 16.70 mm); head width: 2.35–2.55 mm (mean 2.45 mm); head length (with posterior region): 2.96–3.18 mm (mean 3.10 mm). Head, tergites and ventral sclerotized plates of thorax, and abdominal tergites I-VIII dark brown; antennae, maxillae, labium, part of leg above trochanter yellowish brown; thoracic membrane white; coxae, trochanter, and abdominal membrane pale brown, abdominal pleurites and sternites slightly darker than membrane. Head wider than thorax, legs slender, abdominal segment I narrower than segment II, widest at segment III, urogomphi segment I as long as pygopod. — ***Head*** (Fig. 3A–H): Subparallel-sided, about as wide as long, widest at level of stemmata, prognathous with distinct neck; dorsal ecdysial line bifurcate in front 1/3 of head; each side of head with 4 stemmata in a cluster of equal size. Microsculpture on head with front part sparsely furrowed, gradually transitioning backward to scale-like (Fig. 2D, F). Epicranial part (Ep) with 16 pairs of setae, 1 pair of gland (Gl) (Fig. 3C) and 1 pair of pores; posterior area (Pa) with 3 pairs of micro setae (P1–3) and a pair of pores. Ventral side of head with 9 pairs of setae, 1 pair of pores (Fig. 3A), Nasale (Na) (Fig. 4A–C) with 10 pairs of setae, a pair of pores medially, a pair of lateral sensilla (Sm) laterally and a pair of glandular pits posterio-laterally; anterior margin with 9 rounded teeth, paramedian teeth (Pmt) largest, converging toward barely visible median tooth (Mt). Apotome (Ap) triangular, with stalk distinctly extending beyond linear tentorial pits (Tp) (Fig. 3B, E), with 3 pairs of setae, 2 pairs of pores. Epipharynx (Fig. 4D, E) with 3 pairs of olfactory organs each located at ventral side of paramedian teeth and first 2 lateral teeth, 2 bunches of cuticular processes (Cp) separated slightly from each other anteriorly, 1 row of cuticular processes posteriorly. Mandibles slender, with 2 setae at the outer margin and 2 sensillae (1 frontal, 1 lateral). Hypopharynx (Fig. 4D–M) with broad membranous dorsal side

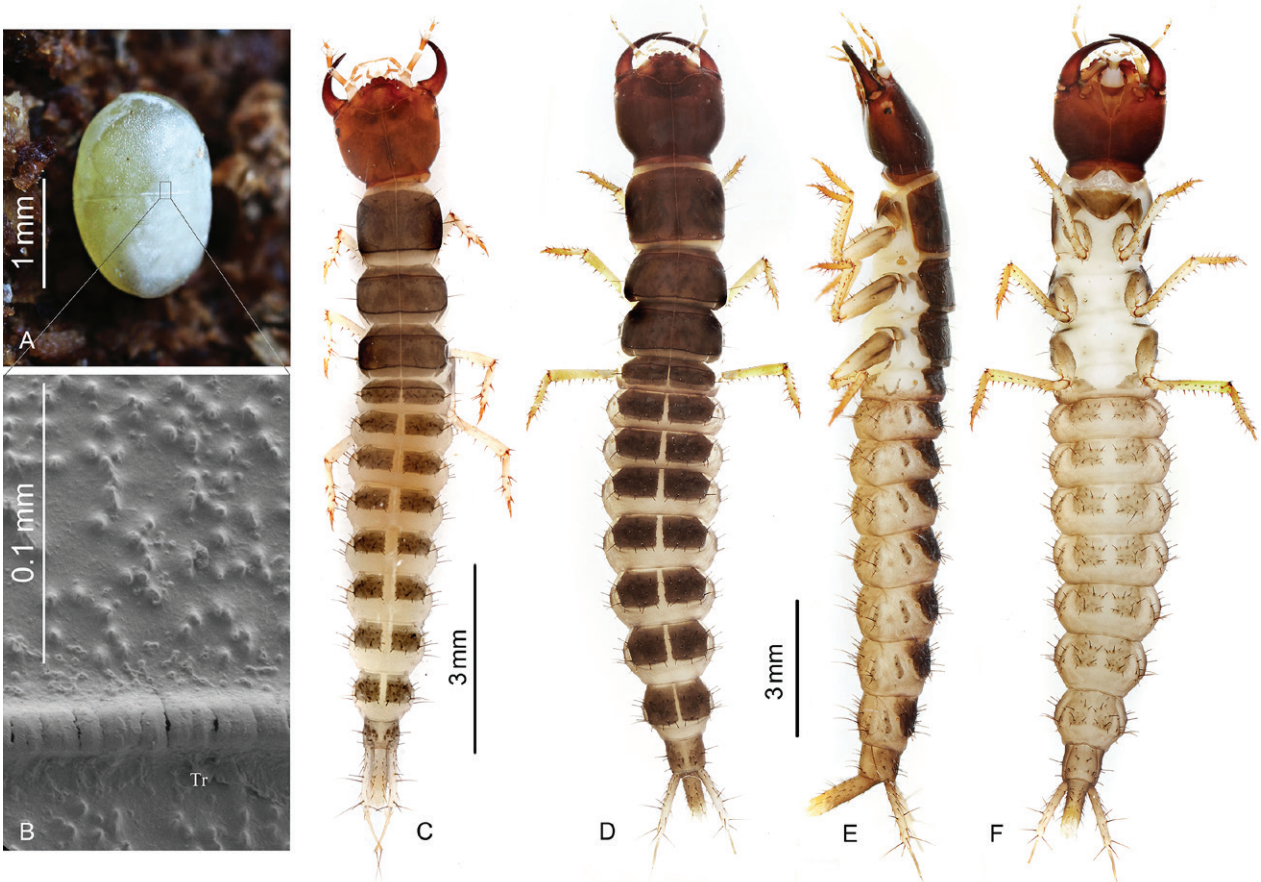

Figure 2. *Algon sphaericollis*. **A** egg; **B** microstructure and transverse ridge of egg; **C** habitus of 1st instar larva; **D**–**F** dorsal, lateral and ventral views of mature larva.

covered with long pubescence (Fig. 4H). Ligula (Fig. 4I, K) conical, distinctly wider at base than segment I of labial palp, margins with a pair of micro setae; sclerotized part of prementum (Pmnt) with 2 pairs of setae (Fig. 4M). Labial palpi (Lp) 3-segmented, length ratio of segments I, II, III = 3.6:3.4:1, respectively; segment I 4.2 times as long as wide, with 1 pore laterally (Fig. 4L); segment II 5.1 times as long as wide, segment III cone-shaped, 3 times as long as wide, tapered subapically, with a few micro sensory appendages apically (Fig. 4G). Antennae (Fig. 5G) 4-segmented, length ratio of segments I-IV = 1:3.6:2.4:1.3, respectively, segment I as wide as long; segment II 6 times as long as wide, with 1 pore ventrally; segment III 6.3 times as long as wide, with 3 macro setae, 2 sensory appendages (Sa) (one conical and the other tiny), 2 solenidia (So) and one pore; segment IV about 4.5 times as long as wide and 3.8 times as long as cone-shaped sensory appendage of segment III, with 3 setae and 4 sol-

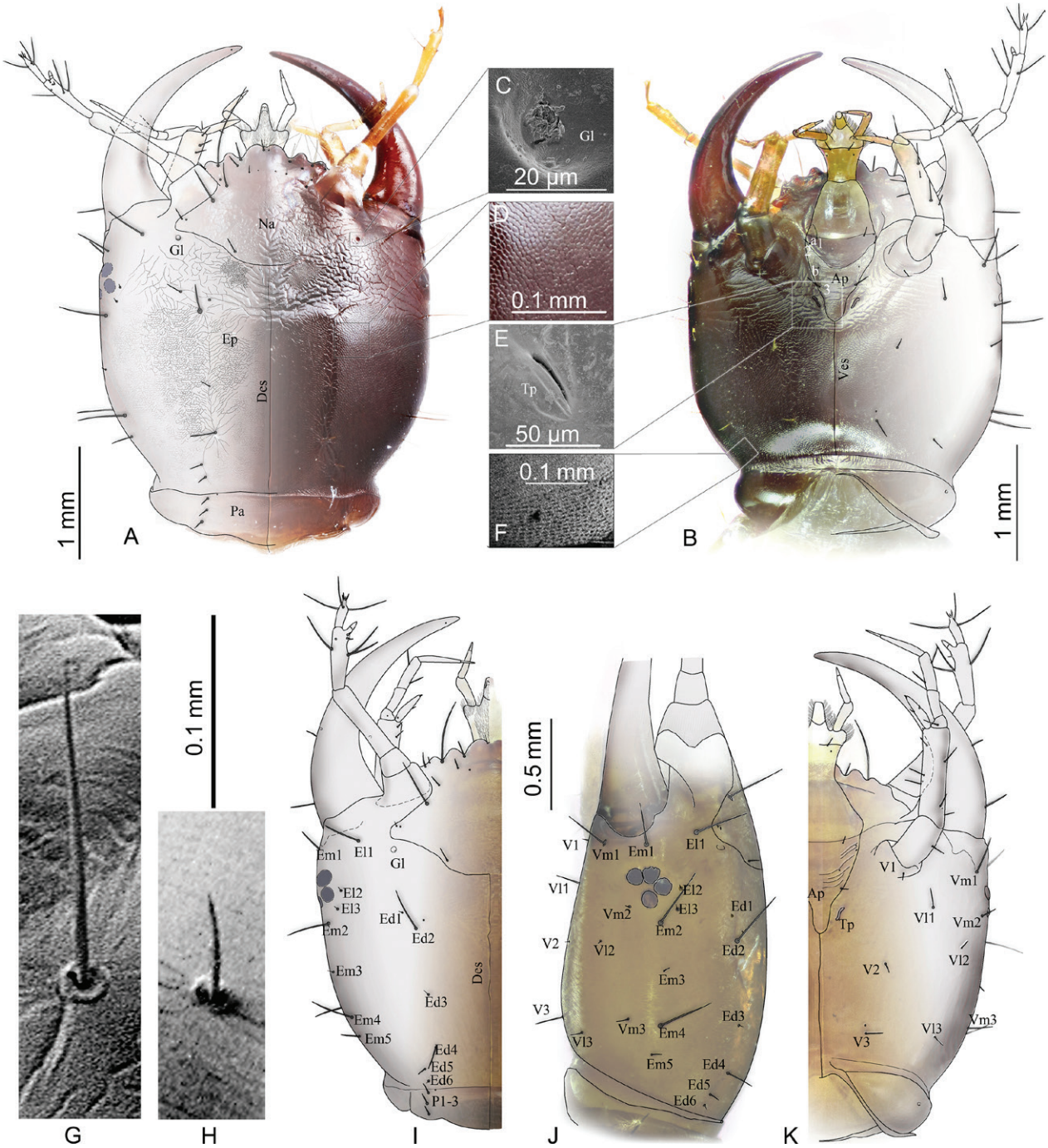

Figure 3. Head of *Algon sphaericollis* larva. A–H: mature larva; I–K: 1st instar larva. **A**, **I** dorsal view; **B**, **K** ventral view; **J** lateral view; **C**–**F** microstructure on dorsal head; **G**–**H** simple setae on head. — Abbreviations: Na, nasale; Ep, epicranial part, Pa, posterior part, Gl, epicranial gland; Ap, apotome; Tp, tentorial pit; Des, dorsal ecdysial suture; Ves, ventral ecdysial suture; Ed, epicranial dorsal seta; El, epicranial lateral seta; Em, epicranial marginal seta; V, ventral seta; Vl, ventral lateral seta; Vm, ventral marginal seta; P, posterior seta.

enidia (So) apically. Maxillae (Fig. 5A–E): length ratio of cardo (Cd): stipes (Stp) = 1:2; cardo 1.5 times as long as wide, bearing 1 seta ventro-laterally; stipes rectangular, 4.2 times as long as wide with 10 setae and 2 pores. Mala (Ma) (Fig. 5C) long, finger-shaped, with 2 setae (1 inner margin and 1 outter margin) and 1 pore, 4 sensory appendages (Fig. 5E) apically; length ratio of mala and segment I of maxillary palpi = 1.15:1. Palpifer with 1 pore and 1 seta ventrally. Maxillary palpi (Pm) 4-segmented; length ratio of segments I–IV = 2.2:2.9:2.8:1, respectively; segments I, II, III, IV 4, 4.8, 7.2, 4.2 times as long as wide, respectively, segment II with 2 setae laterally, segment III with 1 digitiform sensory appendage basally on outer margin, segment IV with a few micro sensory appendages on apex (Fig. 5D). — ***Thorax*** (Figs 6A–J, 7D–I): thoracic chaetotaxy of each instar is identical, thus only the setae of first instar larva (L_1) are coded): Pro-, meso- and metanotum (Fig. 6A, B) with mid-longitudinal

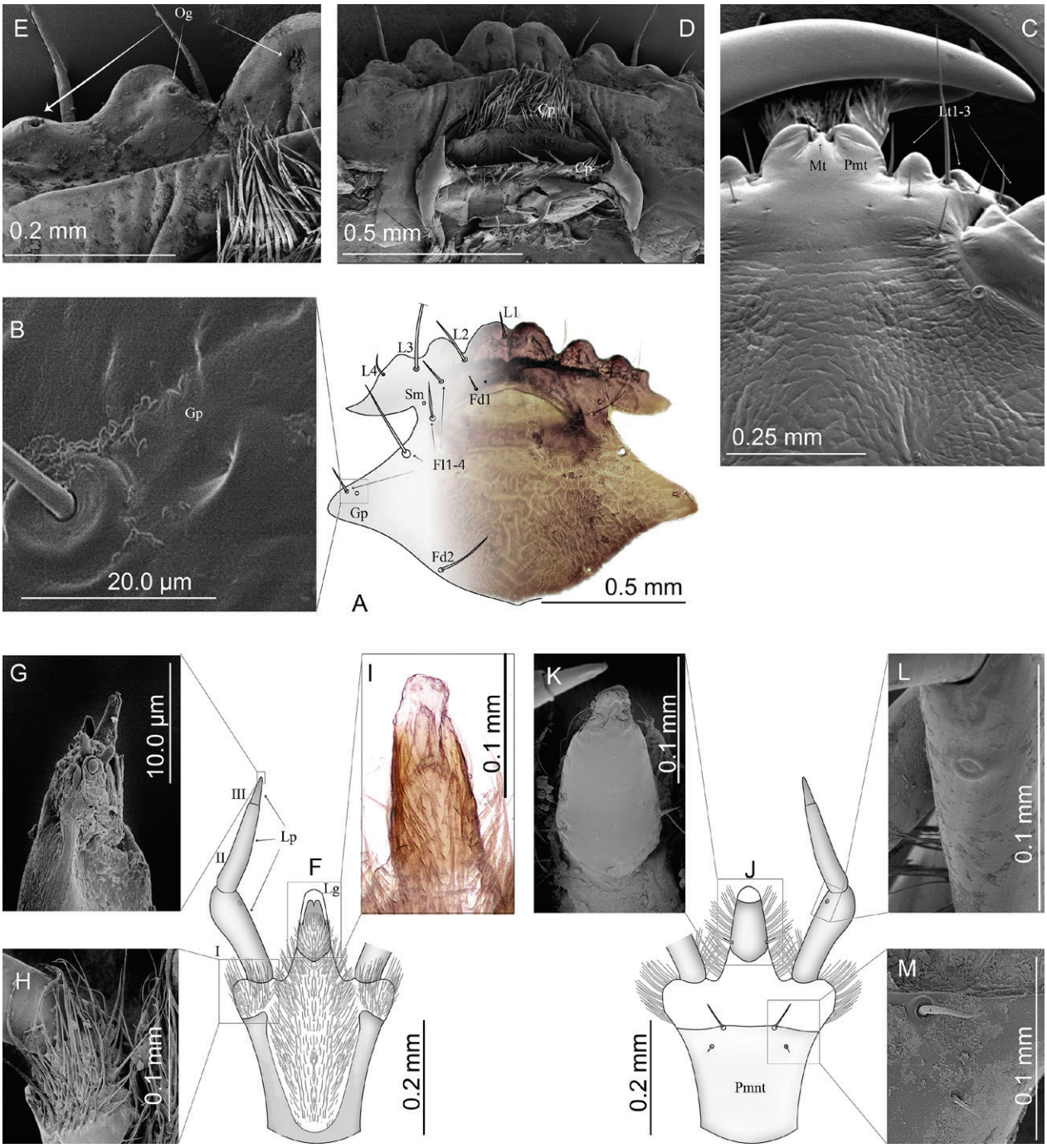

Figure 4. Details of mature larval head of *Algon sphaericollis*. **A** nasale; **B** glandular pit; **C** anterior margin of nasale; **D**, **E** epipharynx; **F** dorsal view of hypopharynx; **G** apex of labial palp; **H** microtrichia; **I**, dorsal view of ligula; **J** ventral view of hypopharynx; **K** ventral view of ligula; **M** setae of prementum; **L** pore of labial palp. — Abbreviations: L, labial setae; Fd, frontal dorsal setae; Fl, frontal lateral setae; Gp, glandular pit; Sm, sensillum; Mt, median tooth, Pmt, paramedian tooth; Lt, lateral teeth; Og, olfactory organ; Cp, cuticular process; Lg, ligula; Lp, labial palp; I–III, segments of labial palp; Pmnt, prementum.

ecdysial line; pronotum with posterior carina (Pc), meso- and metanotum with anterior carina (Ac) and Pc; microstructure of carina as in Fig. 6E. Pronotum (Fig. 6C) slightly wider than long, with 19 pairs of setae (8 macro simple, 1 frayed, 10 micro) and 10 pores and a pair of probably coeloconic sensillum (Cs) (Fig. 6D–G); mesonotum (Fig. 6C) wider than long, chaetotaxy composed of 7 macro simple setae, 2 frayed setae (13, 18), 14 micro

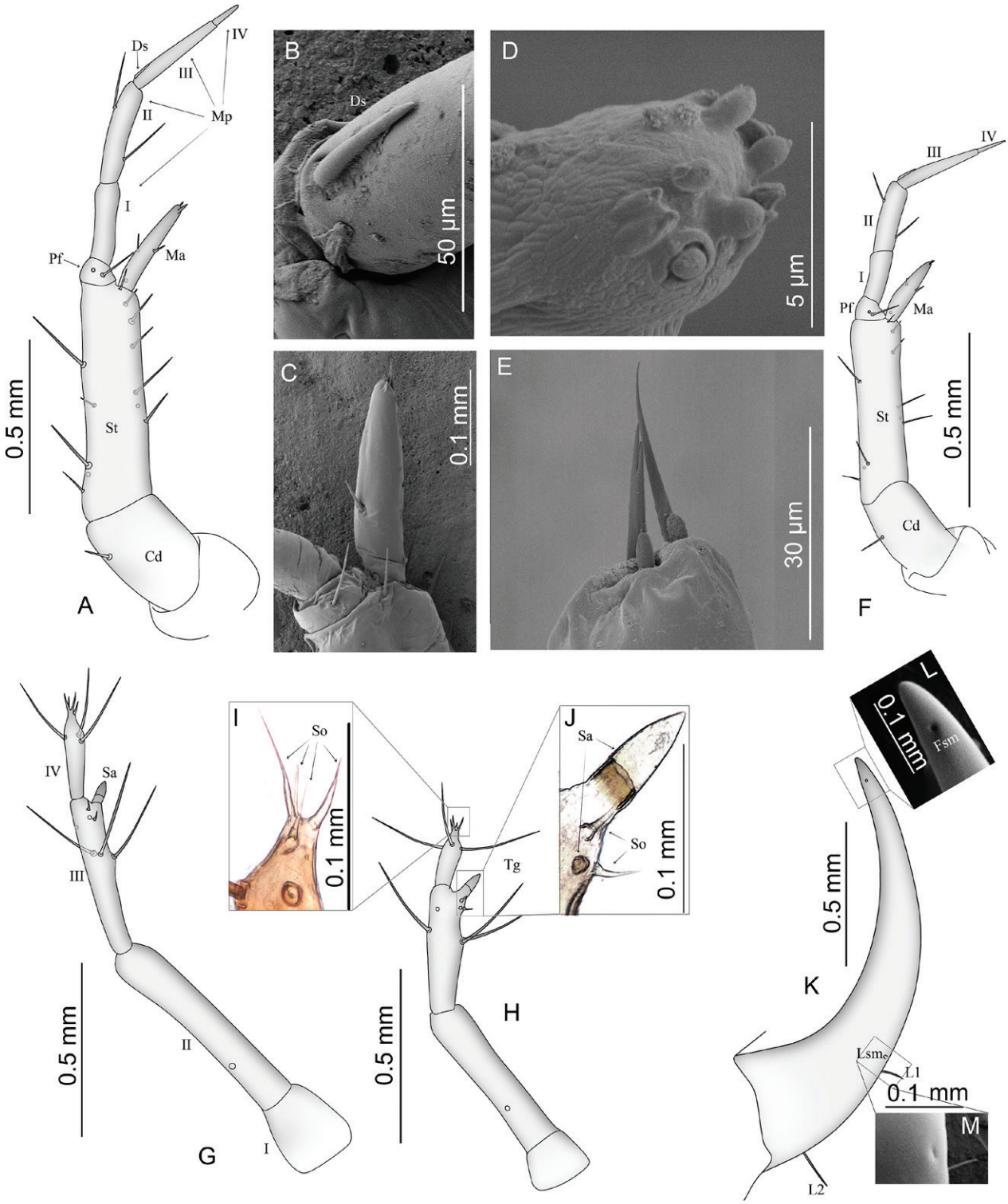

Figure 5. Details of head of *Algon sphaericollis*. F, H–M: 1st larval instar, A–E, G: mature larva. **A**, **G** right maxilla, ventral view; **B** digitiform sensory appendage on segment III of maxilla; **C** mala of left maxilla, ventral view; **D** apex of maxilla; **E** apex of mala; **F**–**H** dorsal view of left antenna; **I** solenidium of segment IV; **J** sensory appendage of segment III; **K** dorsal view of right mandible **L** frontal sensillum; **M** lateral seta and lateral sensillum. — Abbreviations: I–IV, antennal or maxillary segments; Cd, cardo; St, stipes; Lp, labial palp; Ma, mala; Mp, maxillary palp; Pf, palpifer; Ds, digitiform sensory appendage; Sa, sensory appendages; So, solenidium; L1–2, lateral seta; Fsm, frontal sensillum; Lsm, lateral sensillum.

setae (1, 2, 3, 4, 12 situated on cuticle along anterior and lateral margin of tergite), 4 pores and 1 pair of pretergal glands (Ptg). Metanotum similar to mesonotum in chaetotaxy but missing 1 microseta anteriorly. Prothorax ventrally with large triangular cervicosternum (Sc), a pair of episterna (Eps) postero-lateral to cervicosternum, a pair of cuniform lateral sclerites (Ls) between cervicosternum and episterna, and two pairs of small postcoxal sclerites (Pcs) (1 close to the spiracle, the other medially). Cervicosternum with 5 pairs of setae. Episternum, lateral sclerite and postcoxal sclerite each with 1 seta. Ventral side of meso- and metathorax each with a pair of episterna (Eps) and a pair of epimeron (Em) connected by pleural apophysis (Pa). Mesothorax with a pair of small round additional ventral sclerites (Avs) anteriorly, next to episterna, and an islands of small Avs posteriorly each with one micro-seta, next to Pcs, while metathorax without anterior Avs and Pcs, posterior Avs merge into two pieces. Ventral

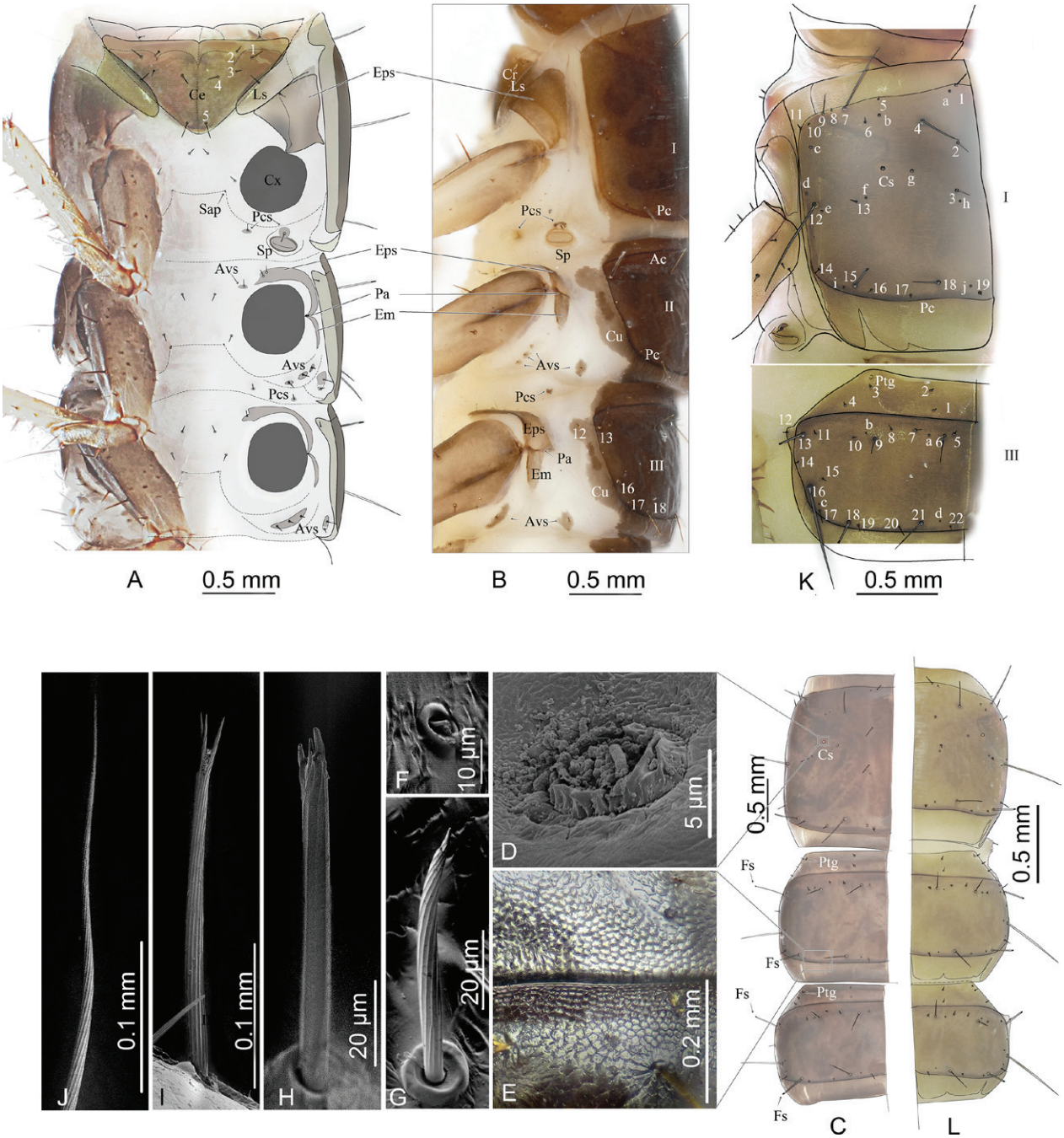

Figure 6. Thorax of *Algon sphaericollis*. K, L: 1st larval instar; A–J: mature larva. **A** ventral view of thorax; **B**, **K** lateral view of thorax; **C**, **L** dorsal view of thorax; **D** gland of pronotum; **E** microstructure of mesonotum; **F**–**G** setae of thorax; **F** microseta on pronotum; **G**, **J** simple seta on pronotum; **H** frayed seta on mesonotum; **I** frayed seta on metanotum. — Abbreviations: Ce, cervicosternum; Ls, lateral sternites; Sap, sternal apophyseal pits; Eps, episternum; Cx, coxa; Sp, spiracle; Pcs, postcoxal sclerites; Avs, additional ventral sclerites; Pa, pleural apophysis; Em, epimeron; Cu, cuticle; Cs, coeloconic sensillum; Ptg, pretergal gland; Ac, anterior carinae; Pc, posterior carinae; Fs, frayed seta. I–III, segments; 1–22, code of setae; a–j, code of pores.

membranous surface of each thoracic segment with a pair of setae (1 medially, the other close to coxa) and a pair of sternal apophyseal pits (Sap). Leg 5-segmented. Fore leg (Fig. 7D–G): length ratio of coxa : trochanter : femur : tibia : tarsungulus = 3.6:1.2:3.5:2.9:1, respectively. Coxa strong, with about 20 setae (6 large) and 2 pores; trochanters (Tr) with several pores and 9 setae, the apical one the largest. Femur (Fe) with about 26 setae; large spine-shaped setae arranged in 2 rows ventrally. Tibia (Tb) slender, with 28 setae, large spine-shaped setae mainly arranged in dorsal and ventral rows, and a comb of bifurcate setae arranged diagonally near apex of anterior aspect (Fig. 7F, G). Tarsungulus (Tu) with 3 spine shaped setae. Mid and hind legs longer than fore leg, with chaetotaxy similar to that of fore leg but without bifurcate setae (Fig. 7H, I). — ***Abdomen*** (Figs 8A–C, 9): segments I–VIII each with divided tergite (Te) and sternite (St), a pair of spiracle (Sp), a pair of paratergites (Pt) and parasternites (Ps) laterally; segment I with transverse carina anteriorly and wide band of more weakly sclerotized cuticles posteriorly, and on segments II–VIII the cuticle bands gradually narrow and disappear. Spiracles of segment I larger

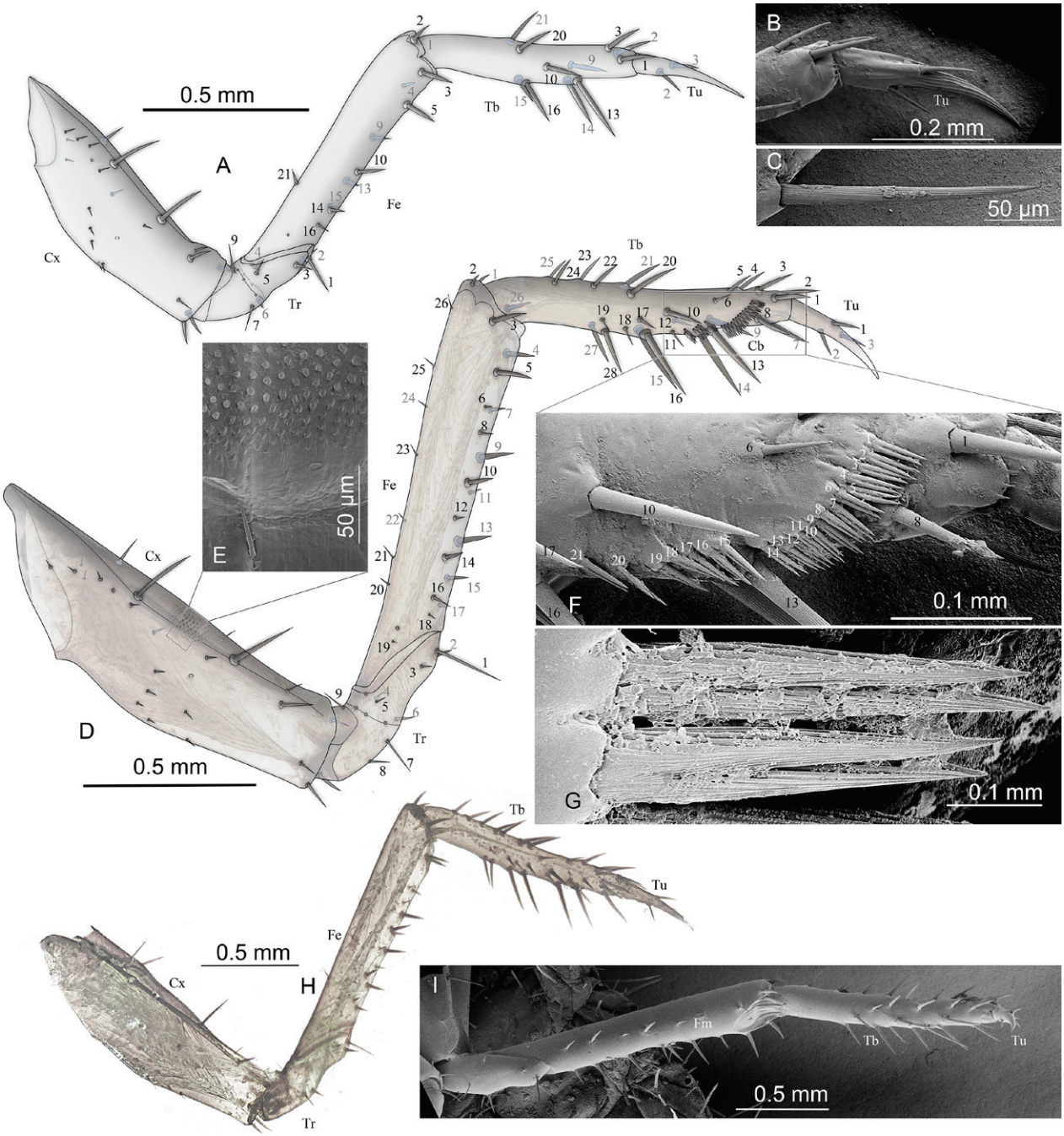

Figure 7. Legs of *Algon sphaericollis*. A–C: 1st larval instar; D–I: mature larva. **A**, **D** fore left leg in anterior aspect; **B** tarsungulus in posterior aspect; **C** spine on tibia; **E** microstrucure of fore coxa; **F**, **G** comb of bifurcated setae on tibia; **H** middle left leg in anterior aspect; **I** hind left leg in anterior aspect. — Abbreviations: Cx, coxa; Tr, trochanter; Fe, femur; Tb, tibia; Tu, tarsungulus; Cb, comb. 1–26, code of setae (the gray codes represent the setae of the posterior aspect).

than spiracles of segments II–VIII. On segment I paratergites and parasternites posteriorly fused to form U-shaped lateral sclerites (Fig 8B), paratergites of segment II–VIII divided into a main part and an additional lateral sclerites. Segment I: tergite with 23 pairs of setae (10 macro club-shaped, 13 micro simple) and 6 pores; sternites with 14 pairs of setae (9 macro and club-shaped, 5 micro and simple) and one pore; paratertites and parasternites with 7 setae (3 macro and club-shaped); segments II–VIII: tergites with 23 pairs of setae (10 macro club-shaped, 7 medium sized club-shaped, 14 simple and micro); sternites with 16 pairs of setae (2 macro and simple, other frayed or club-shaped) and 5 pairs of pores; paratergites with 5 setae (3 club-shaped and 2 micro) on the big sclerite and 1 club shaped seta on the small one; parasternites with 7 setae (6 club-shaped and 1 micro). Type of

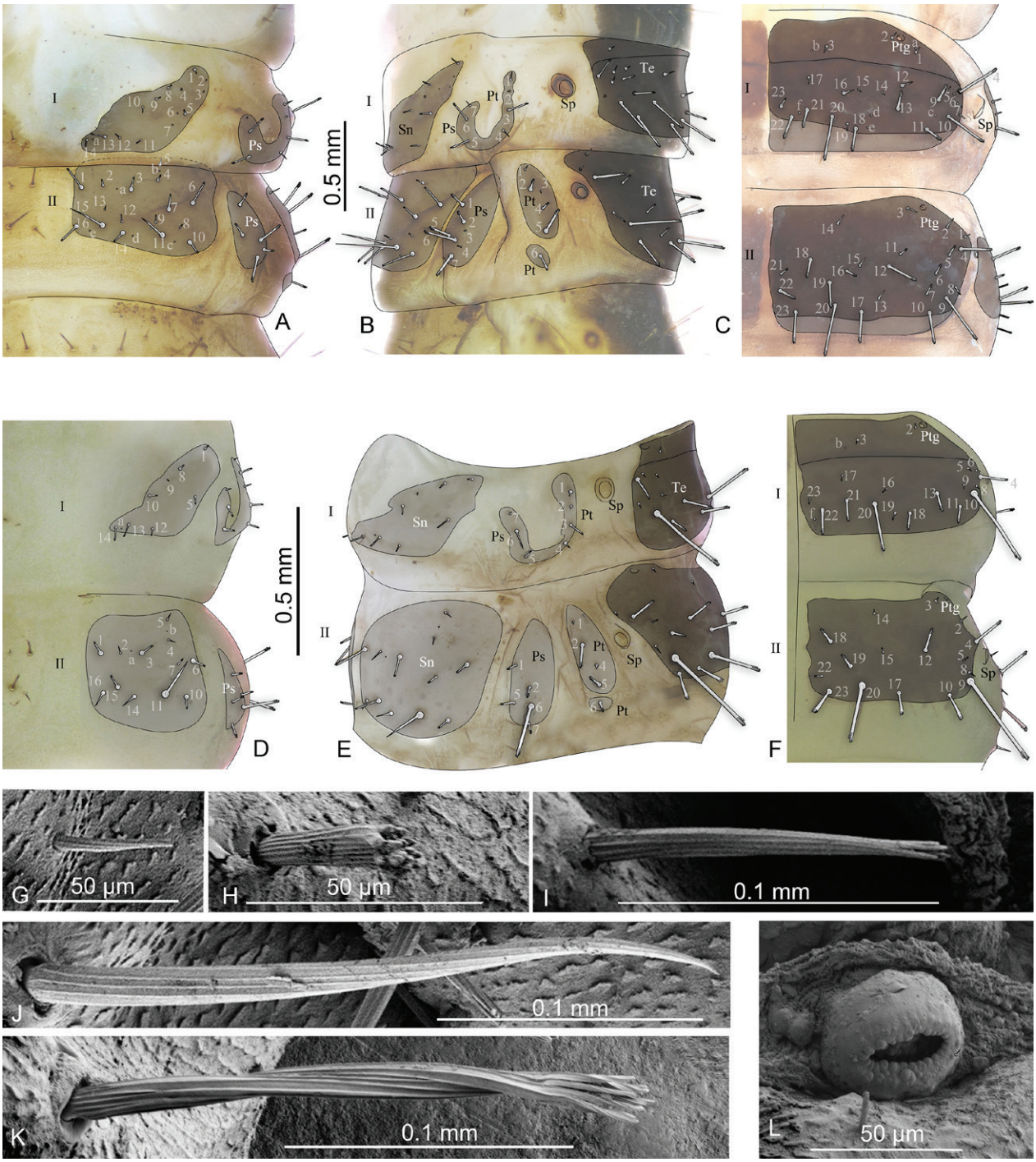

Figure 8. Abdominal segments of *Algon sphaericollis*. D–L: 1st larval instar; A–C: mature larva. **A**, **D** left abdominal sternites I and II; **B**, **E** left side of abdominal segment I and II, lateral; **C**, **F** right abdominal tergite I and II; **G**–**K** types of setae of abdominal sternite; **G** simple micro seta; **H** club-shaped seta; **I** long frayed seta; **J** long simple seta; **K** long, frayed seta of abdominal tergite; **L** spiracle of abdominal segment II. — Abbreviations: Te, tergite; Sn, sternite; Pt, paratergite; Ps, parasternite; Sp, spiracle; Ptg, pretergal gland. I, II, segments. 1–26, code of setae; a–f, code of pores.

setae on abdominal segments as on Fig. 8G–K. Abdominal segment IX with 10 pairs of setae (4 club-shaped and 6 micro) on tergite and 6 pairs of setae on sternite (1 club-shaped, other simple), with two long, articulated, 2-segmented urogomphi (Fig. 9). Segment I of urogomphi about twice as long as abdominal segment IX, with about 20 setae, 2 of them frayed (Fig. 9G), segment II slender, about half as long as segment I, with two simple setae, (one long, the other much shorter) at apex. Surface of urogomphi with numerous tiny stylus (Fig. 9C). Abdominal segment X (pygopod) about as long as segment I of urogomphi, with about 26 pairs of setae, many of which frayed (Fig. 9F). Surface of pygopod with numerous sharp cuticular protuberance (Fig. 9B).

First instar larva (L_1) (only characters listed that are different from those of mature larva)**.** Body length: 9.1–12.0 mm (mean 10.3 mm); head width: 1.69–2.01 mm (mean 1.95 mm); head length: 1.79–2.18 mm (mean 2.15 mm). Head reddish brown, tergites and ventral sclerotized plates of thorax, and abdominal tergites I–VIII brown (Fig. 2C). — ***Head*** (Fig. 3I–K): inverted trapezoid, widest at level above stemmata then tapering towards neck, chaetotaxy as in Fig. 3I–K (same as in mature larva); microsculpture on head not as distinct as mature larva. Length ratio of antennomeres (Fig. 5H–J) I–IV = 1:3.4:2.7:1.2, segment IV about 3.2 times as long as wide and 2.2 times as long as cone-shaped sensory appendage of segment III, Maxillae (Fig. 5F): cardo 2 times as long as wide, stipes with 8 setae and 2 pores. Length ratio of mala and segment I of maxillary palpi = 1.3:1. length ratio of segments I–IV of maxillary palpi (Pm) = 1.7:2.8:2.3:1, respectively; segments I, II, III, IV 3.2, 4.2, 7.2, 4.2 times as long as wide. Mandible similar to that of mature larva (Fig. 5K–M). — ***Thorax*** (Fig. 6K, L): structure and chaetotaxy of thoracic segments similar to that of mature larva. Fore legs (Fig. 7A–C) slightly thicker than in mature larva, length ratio of procoxa : trochanter : femur : tibia : tarsungulus = 2.1:0.85:2.0:1.75:1, respectively. Setae of femur and tibia much less than in mature larva, fore tibia without bifurcate setae. — ***Abdomen*** (Fig. 8D–F): tergites I–VIII without weakly sclerotized cuticle band posteriorly present in L_3; number of macro club-shaped setae of tergite I same as in L_3 (4, 10, 11, 13, 18, 19, 20, 21, 22, 23), simple setae less than in L_3, macro club-shaped setae of tergite II–VIII identicle to L_3 (4, 9, 10, 12, 17, 18, 19, 20, 22, 23), other setae less than in L_3. Sternite I with same club-shaped setae as L_3, without micro setae; segment II lack of the central area setae (8, 9, 12, 13) present in L_3. Paratertites and parasternites (Fig. 8E) of segment I identical to L_3, segment II missing 1 and 2 setae on paratergites and parasternite, respectively. Segment IX and X similar to that of L_3.

Pupa (Fig. 10)**.** Colour orange, cuticula well sclerotized. Body length (without terminal process): 8.86–10.21 mm

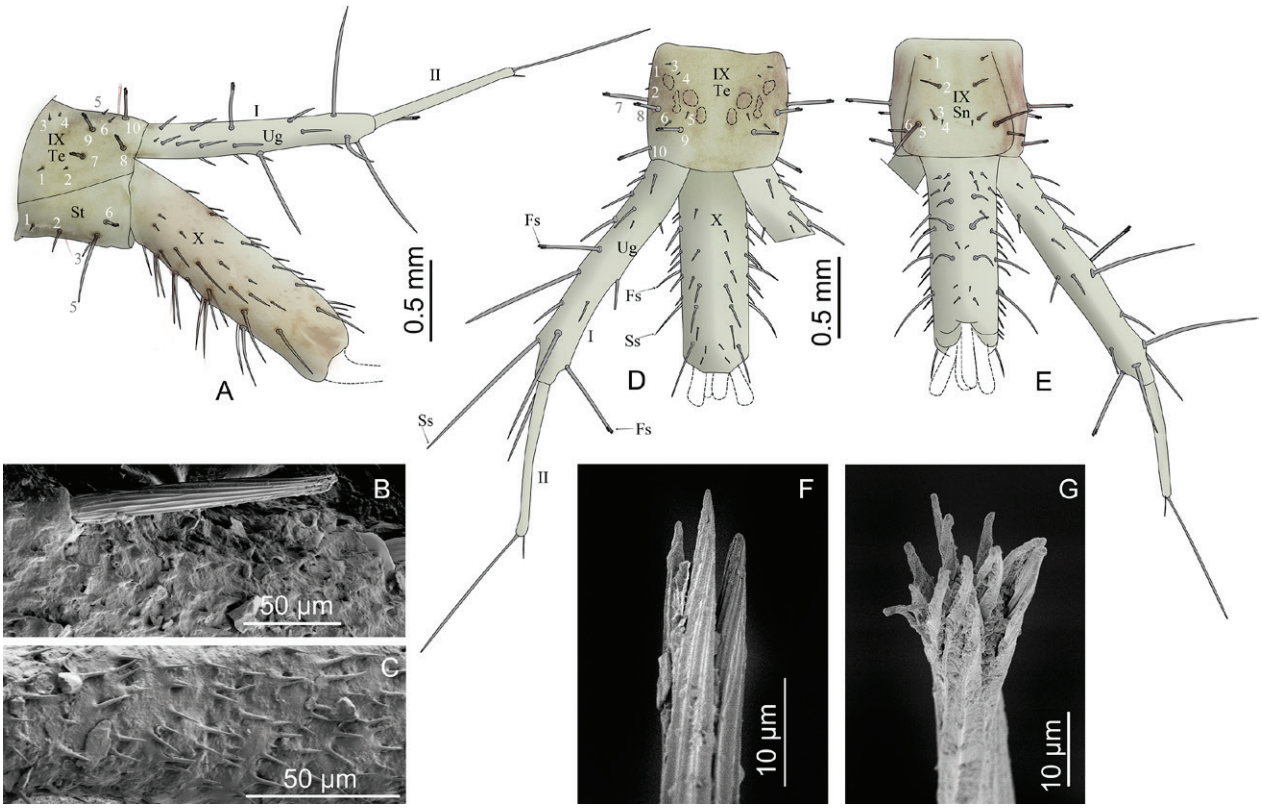

Figure 9. Abdominal segments IX, X and urogomphi of mature larva of *Algon sphaericollis*. **A** lateral aspect; **D** dorsal aspect; **E** ventral aspect; **B** microstructure of abdominal segment X; **C** microstructure of urogomphi; **F** apex of frayed seta on segment X; **G** apex of frayed seta on urogomphi. — Abbreviations: Te, tergite; Sn, sternite; Pt, paratergite; Ug, urogomphi; Ss, simple seta; Fs, frayed seta. 1–10, code of setae.

(mean 9.90 mm); body width in the widest place (between hind knees): 4.2–4.5 mm (mean 4.35 mm); head width (between eyes): 2.2–2.7 mm (mean 2.56 mm); head length: 3.2–3.6 mm (mean 3.4 mm); pronotum width: 3.0–3.3 mm (mean 3.18 mm); pronotum length: 2.7–3.0 mm (mean 2.9 mm). Mandibles crossed at apices. Antennae curved, protruding slightly beyond half-length of elytra. Anterior margin of pronotum with 16 setiform projections, about half of pronotum length. Surface of pronotum uneven, with a pair of pores subantero-laterally (Fig. 10D). Wings reaching posterior margin of abdominal segment III. Meso- and metatibiae with about 16 and 6 protuberances, respectively. Protarsi reaching level of apices of maxillary palps, mesotarsi almost reaching level of apices of wings, metatarsi protruding slightly beyond anterior margin of abdominal segment VII. Abdomen moderately and gradually widening to segment IV and then tapering to terminal segment of the body. Abdominal tergite I twice as long as tergite II. Abdominal segments VII and VIII each bearing on sides a pair of long, curved, setiform projections, projections on segment VII longer than those on VIII. Terminal sternite with well-marked sexual dimorphism (Fig. 10E, F). Female pupa (Fig. 10F) with double gonotheca (Gt) and ventral prolongations (Vp); male pupa (Fig. 10E) with single gonotheca; terminal prolongation of both sexes with straight accessory

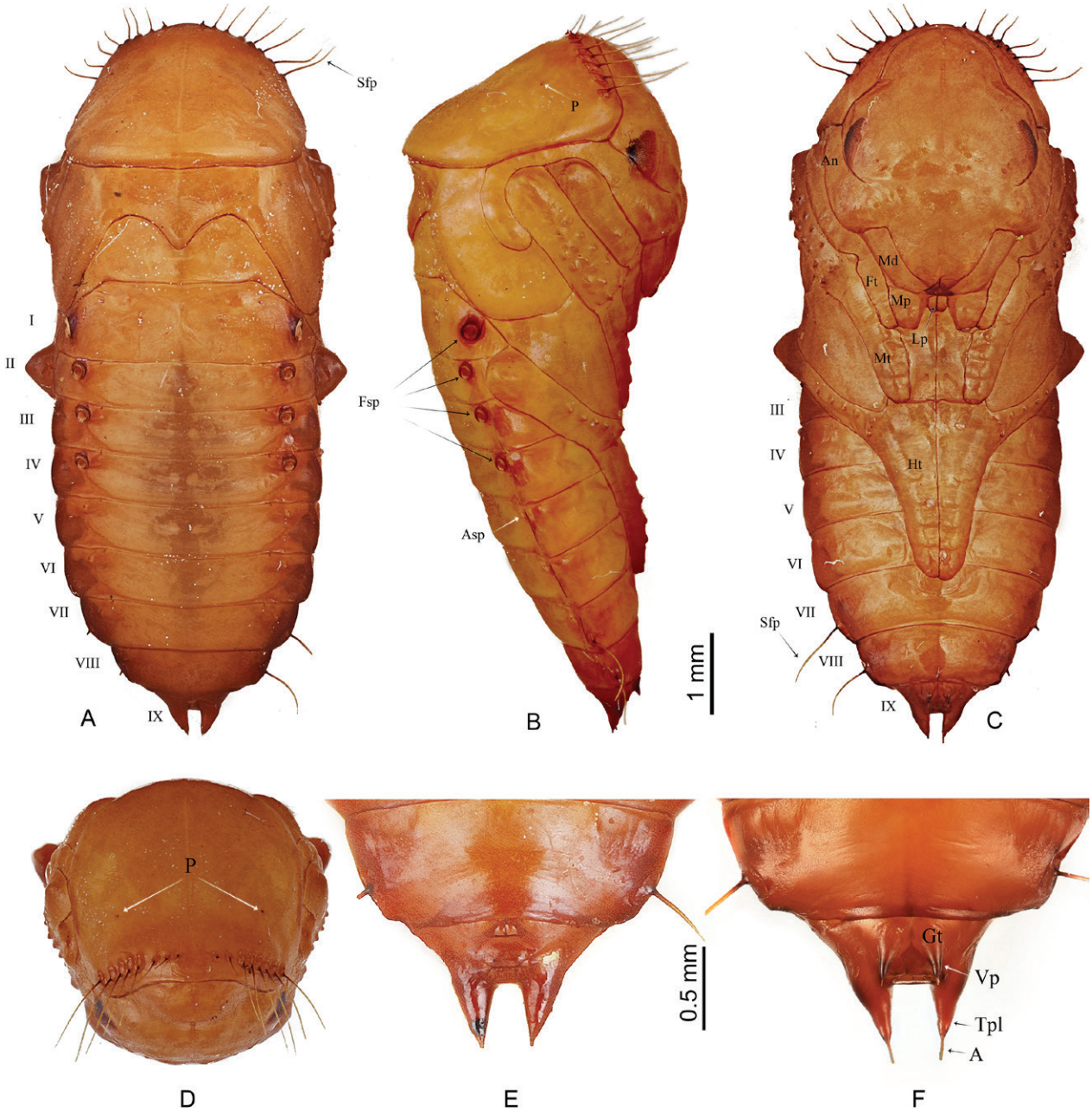

Figure 10. Pupa of *Algon sphaericollis*. **A** dorsal aspect; **B** lateral aspect; **C** ventral aspect; **D** frontal aspect; **E** male terminal sternite; **F** female terminal sternite. — Abbreviations: An, antenna; Asp, atrophied spiracle; Fsp, functional spiracle; Ft, fore tarsus; Md, mandible; Mp, maxillary palp, Lp, labial palp; Mt, mid tarsus; Ht, hind tarsus; Sfp, setiform projection; P, pore; Gt, gonotheca; Vp, ventral prolongation; Tpl, terminal prolongation; A, accesory; I–IX, abdominal segments.

(A) with apex rounded (Fig. 10E, F, apex of male broken off). Abdominal tergites I–IV with functional spiracles, tergites V–VIII with atrophied spiracles (Fig. 10B).

3.2. Morphology of immature stages of other reared species of Staphylinini

The morphology of six Staphylinini species was studied using the same methods as employed for *Algon sphaericollis*. Photographs of selected species, which were not described in detail but were solely utilized for phylogenetic analysis and morphological comparisons in this study, can be found in Figs 11 and 12.

3.3. Results of phylogenetic analyses

The analysis, based on immature stages, which included characters of egg, larva, and pupa, yielded 841 most parsimonious trees with the length of 230 steps. The strict consensus tree (Fig. 13A) revealed monophyletic Tanygnathinini, Acylophorini and Staphylinini. The other tribes, such as Quediini represented by 4 species, and Amblyopinini represented by 3 species, were not retrieved. *Natalignathus* was strongly supported as the sister group of Tanygnathinini, which corresponds to its speculated position proposed by Shaw et al. (2020). The placement of *Quedius antipodum* within Amblyopinini was previously supported by adult characters and DNA (Shaw et al. 2020). However, the larval data do not sup-

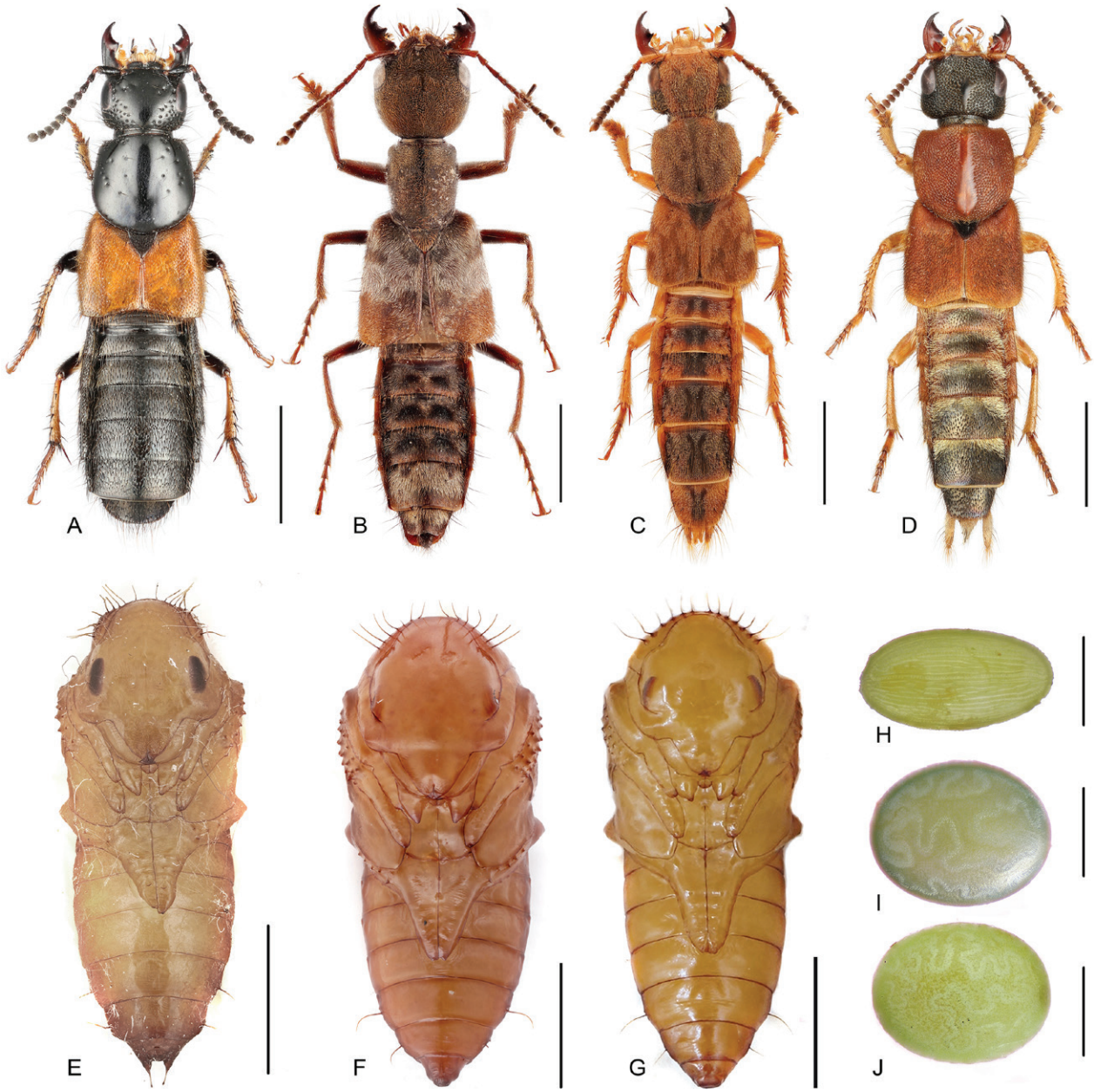

Figure 11. Species with immature data obtained by rearing in the laboratory. A–D: habitus of adults; E–G: pupae; H–J: eggs. **A**, **E**, **H** *Philonthus spinipes* Sharp, 1874; **B** *Eucibdelus* sp.; **C**, **F**, **I** *Platydracus marmorellus* (Fauvel, 1895); **D**, **G**, **J** *Saniderus* sp. Scale bars: A–G, 3 mm; H–J, 1 mm.

port this conclusion, as was the case in the study by Pietrykowska et al. (2014), and strongly support the placement of *Q. antipodum* in Staphylinini. The relationships between tribes remained unresolved, but Acylophorini were supported as the sister group of *Antimerus* + *Astrapaeus*. Within the Staphylinini, the monophyly of Philonthina and Staphylinina was supported, but the internal topology within these subtribes remained unresolved. The

Figure 12. Larvae of species with immature data obtained by rearing in the laboratory. **A**–**C** *Philonthus spinipes* Sharp, 1874; **D**–**F** *Eucibdelus* sp.; **G**–**I** *Platydracus marmorellus* (Fauvel, 1895); **J**–**L** *Saniderus* sp. Scale bars: 3 mm.

50% majority rules consensus tree corresponds well to the strict consensus tree based on DNA and adult morphology by Chani-Posse et al. 2018 (Fig. 14A, B) in the position of Tanygnathinini, Amblyopinini, and Erichsonini as the early-branching groups and a strong support for Staphylinini as the crown group.

The analysis, based solely on 53 larval characters, found 333 trees with the length of 190 steps (Fig. 13B). Only Tanygnathinini (including *Natalignathus*) and Acylophorini were resolved at the tribe level. Staphylinini, Philonthina, and Staphylinina were not resolved. Additionaly, a clade including *Abemus*, *Emus*, *Ontholestes*, *Platydracus* and *Saniderus* emerged. This is consistent with previous studies grouping these genera together as the *Platydracus* group based on adult characteristics (Chani-Posse et al. 2019) or the combination of morphology and DNA (Brunke and Smetana 2019). When characters are mapped on the 50% majority rule consensus tree, it becomes evident that early branching clades possess numerous larval synapomorphies, while crown group members predominantly exhibit synapomorphies in pupae or eggs (Fig. 15). Tanygnathinini are characterized by posteriorly placed tentorial pits on the larval head capsule (character 10-2, Fig. 15A), and the spiracle append-

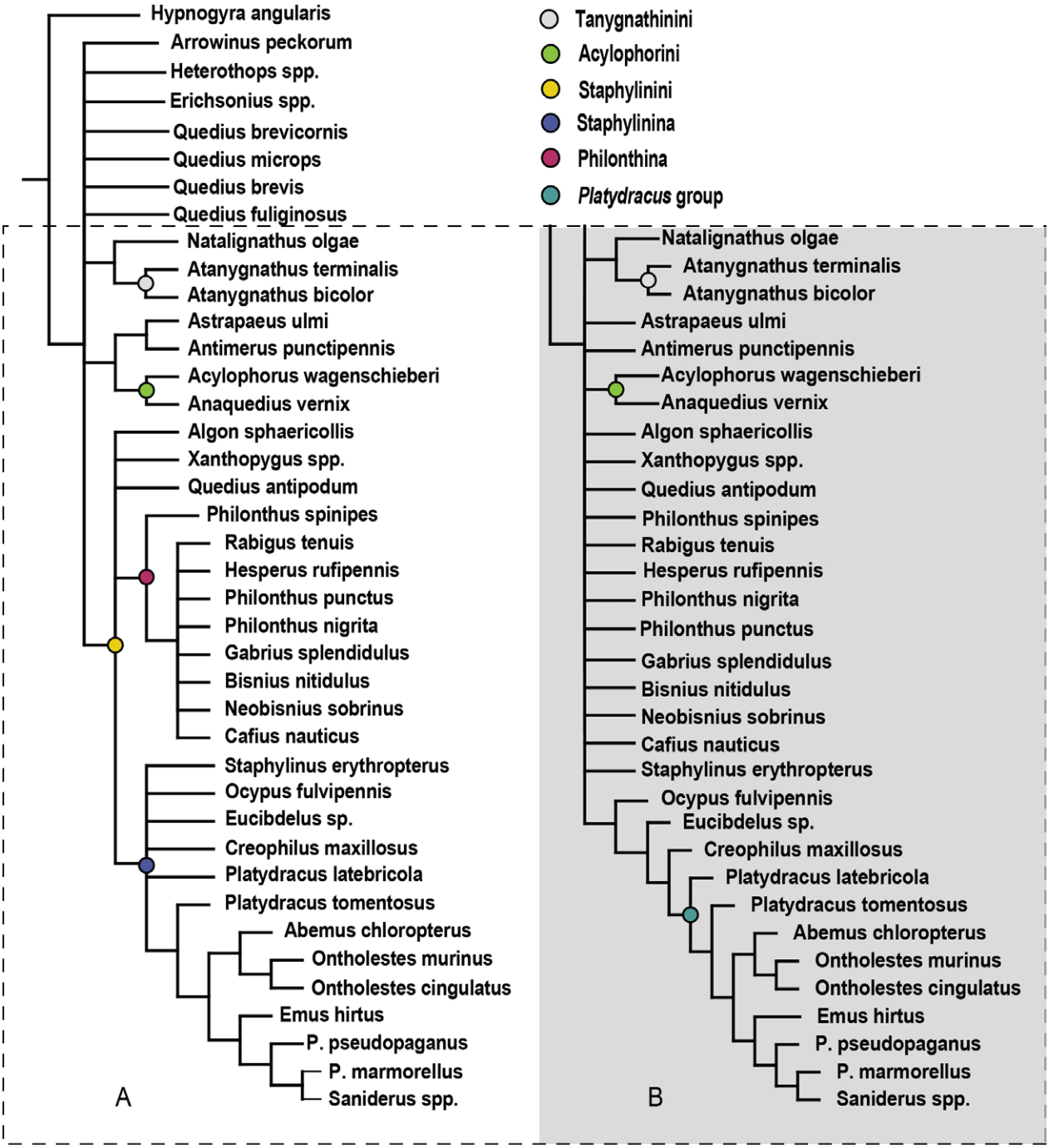

Figure 13. Strict consensus of trees recovered by maximum parsimony using TNT for the immature morphological data of **A** 71 characters including egg, larva and pupa; **B** 53 characters of larvae.

age on the prothorax (character 32-1). Acylophorini can be identified by an anteriorly placed digitiform sensory appendage on maxillae (character 21-1, Fig. 15J). Pupal characters that distinguish Staphylinini from other tribes encompass setiform projections on the pronotum (character 62-0, Fig. 15F) and the sides of abdominal segments (character 66-0, Fig. 15G). Additionally, the apex of apical accessories on the terminal prolongations of segment IX is not pointed (character 70-1) in most species. The presence of uniquely curved apical accessories on the terminal prolongations of segment IX is a distinctive feature found exclusively in pupae of Staphylinina (character 69-1, Fig. 15P). The absence of terminal prolongations appears to be a potential synapomorphy of pupae of the *Platydracus* group, although further investigation is needed. The clades with strong support of pupal characters revealed by us correspond to those revealed by Staniec and Pietrykowska-Tudruj (2019) solely on pupal data. Eggs with longitudinally arranged rows of aeropyles are exclusively found in the Philonthina (character 3-1, Fig. 15K) and densely distributed aeropyles forming a band are exclusive for the Staphylinina (character 3-3, Fig. 15O). Interestingly, this band appears as an equatorial feature in *Creophilus*, *Ocypus* and *Eucibdelus* but transforms into a wave-like pattern in *Staphylinus* (Hinton, 1981). In most members of the *Platydracus* group, it forms an unbroken wave-like band, with the density of the wave varying among species and genera.

These findings suggest that, with the exception of highly derived groups such as Tanygnathinini, Acylophorini, and the *Platydracus* group, similar larval characters evolved or were lost multiple times in parallel, which diminish their phylogenetic signal. We speculate that the absence of egg and pupal data led to the placement of *Quedius antipodum* within Staphylinini in our analyses. Previous studies have found numerous larval characters useful for subtribe-level or even species-level idetification of the Staphylininae species (Kasule 1970; Staniec

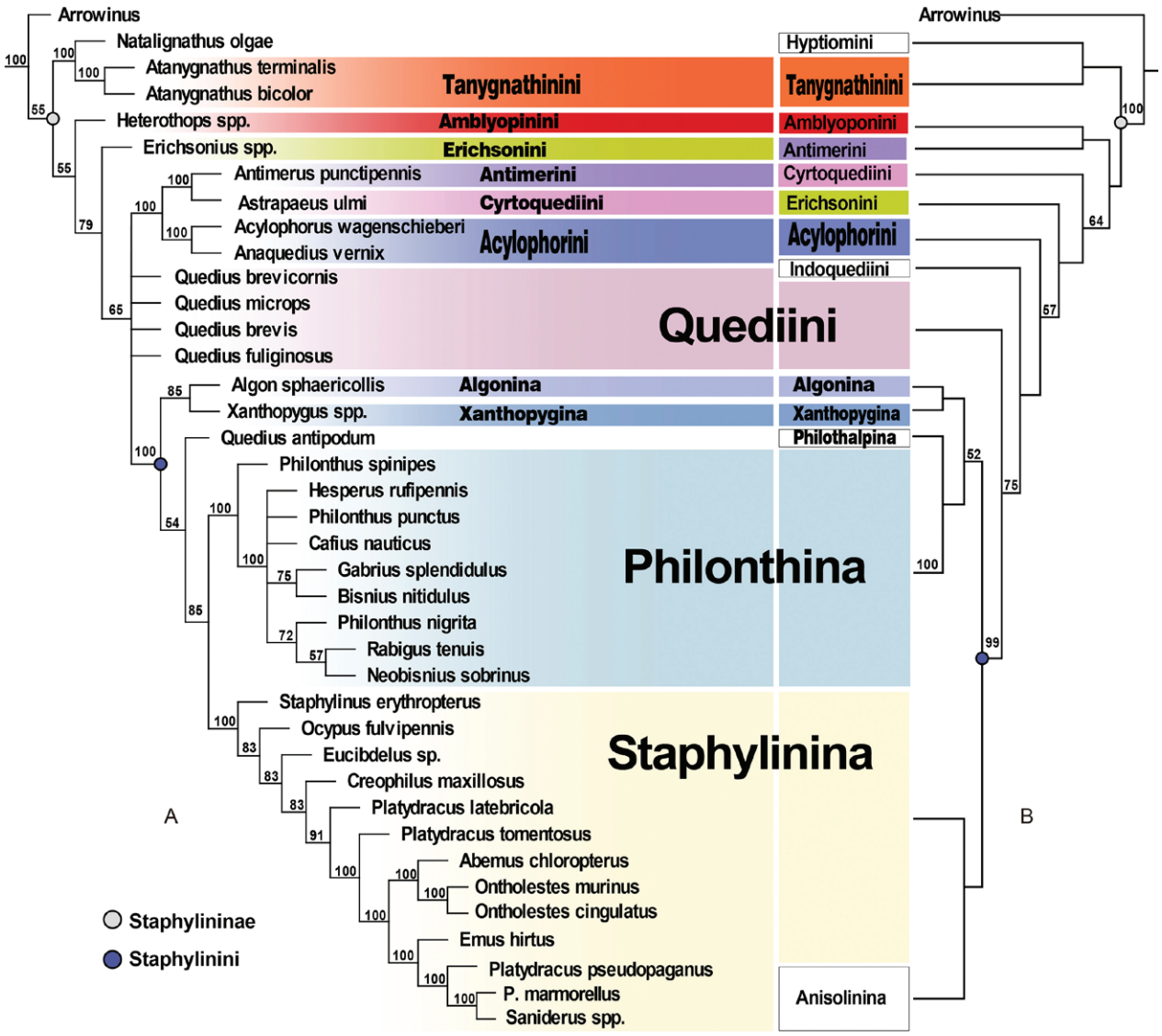

Figure 14. Topological congruence between **A** 50% majority-rule consensus of 841 MP trees using TNT for the immature morphological dataset of 71 characters and **B** strict consensus of 23 MP trees using TNT for a combined dataset of DNA and adult morphlogies by Chani-Posse et al. (2018) (simplified).

2005b; Pietrykowska-Tudruj et al. 2014). In this study, we tested the phylogenetic significance of these characters and found that most are non-homologous traits, significant only when combined with others.

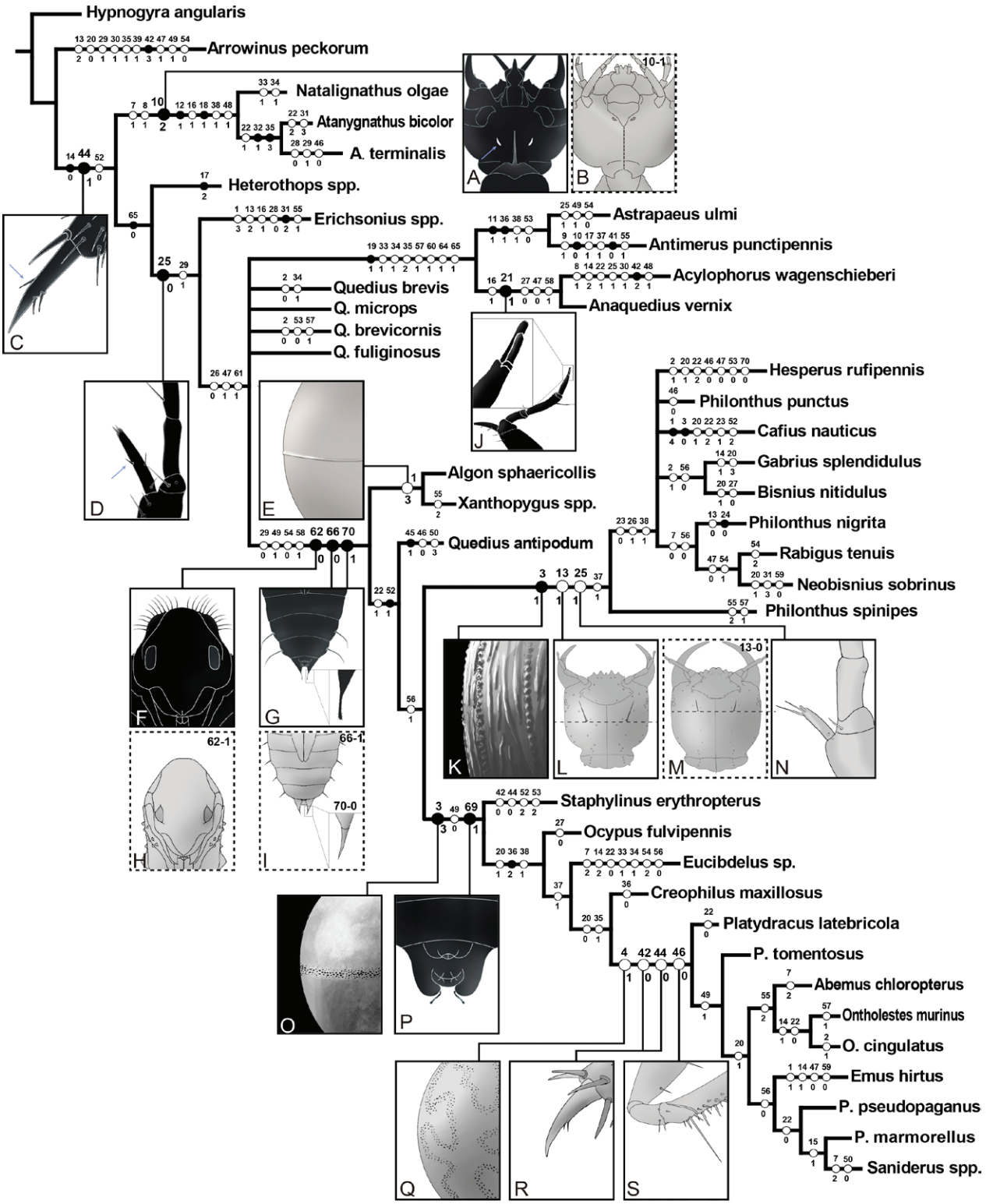

Figure 15. Phylogenetic analysis with unambiguously optimized character changes plotted along internodes of 50% majority-rule consensus MP tree for the immature morphological dataset. Character numbers are above circles, state numbers are below circles. Black circles indicate unique synapomorphies, white circles indicate homoplasies, both are indicated by morphological illustrations of representative species including: **A** *Atanygnathus terminalis* (after Staniec 2005b); **B**, **O** *Eucibdelus* sp.; **C**, **D**, **E**, **M** *Algon sphaericollis*; **F**, **G**, **K** *Philonthus spinipes*; **Q**, **R**, **S** *Platydracus marmorellus*; **P** *Staphylinus erythropterus* (after Pietrykowska-Tudruj and Staniec 2012); **L**, **N** *Philonthus punctus* (after Staniec and Pietrykowska-Tudruj 2006); **H**, **I** *Quedius brevicornis* (after Staniec 2003); **J** *Anaquedius vernix* (after LeSage 1984).

We focus on novel characters of potential phylogenetic importance, which may offer new insights into evolutionary connections. The presence of spine-like setae on the dorsal side of the tarsungulus (character 44-1, Fig. 15C) represents a synapomorphy of Staphylininae, as previously documented by Solodovnikov and Newton (2005). Notably, this trait is absent in *Staphylinus*, *Platydracus* group (44-0, Fig. 15R) and the outgroups, suggesting a potential reversal to the ancestral condition. The epicranial dorsal macrosetae (Ed2) situated at the mesoanterior region of the head in most Staphylininae (character 13-0, Fig. 15M) have shifted to the mesoposterior part of the head in many members of Philonthina (character 13-1, Fig. 15L). The presence of microsetae on the inner and outer margins of the mala (character 25-0, Fig. 15D) is common in Staphylininae of the Northern hemisphere clades, with exceptions of *Acylophorus* and *Astrapaeus*. However, these microsetae are notably absent in Philonthina (character 25-1, Fig. 15N). The spine-like macroseta on the ventral front face of the foreleg trochanter is exceptionally elongated in the *Platydracus* group (character 46-0, Fig. 15S), this feature is also present in *Hypnogyra*, an outgroup of Staphylininae.

3.4. Evolution of larval characteristics

Our analyses indicate that larval morpohlogy of the Staphylininae is a mosaic combination of homologous and analogous characters. It can be illustrated by the setae and other structures on the protibia. Boháč (1982) defined two morpho-ecological types of protibia for Staphylinina, the running and burrowing type. We extend this concept here to the whole Staphylininae and propose three protibial types:

(1) The running type: Protibiae are moderately long and slender (length : width ratio is 4–6), with parallel sides c. in basal two-thirds or with a slight dilatation at mid-length (Fig. 16A). This type is prevalent in early-branching and crown groups, particularly in Quediini and the majority of Staphylinini.

(2) The elongate running type: Protibiae are nearly as long as femora (length : width ratio > 6), widest near the base and gradually tapering towards apex (Fig. 16C). This type is more common in early-branching groups like Acylophorini, *Astrapaeus*, and Tanygnathinini. The shape is a bit modified in Tanygnathini: the protibial is slightly dilatated in the basal third and tapers suddenly towards the apex.

(3) The burrowing type: Protibiae short and wide, of the tubular shape (length : width ratio < 4), with an apical dilatation and dense coverage with prominent spines (Fig. 16B). Boháč (1982) originally observed this type in *Platydracus*, *Ontholestes* and *Abemus*, here we found it present in all members of the *Platydracus* group. Interestingly, a similar morphological adaptation is present in *Arrowinus* of Platyprosopinae, possibly indicating a case of convergent evolution.

The presence of bifurcate setae on the anterior aspect of the protibia is considered a plesiomorphic trait within Staphylininae (Pietrykowska-Tudruj et al. 2014) and its nearest relative, *Arrowinus*. Another supposedly plesiomorphic trait observed in Staphylininae and the closely related Xantholininae, is the comb-like structure composed of tiny setae arranged in lines or clusters on the tibia (Fig. 16F; for other species in Xantholininae, see Kasule 1970). Interestingly, the tiny setae constituting the comb are frequently substituted by bifurcate setae (Fig. 16G). Notably, these traits are subject to collective or individual loss within different taxa over evolutionary time. Classification based on tibial shape, comb presence, bifurcate setae presence, and bifurcate setae within the comb yields nine observed combinations (Fig. 16A–C). Of the taxa with the elongate running protibiae, Tanygnathinini lose both the comb and bifurcate setae. *Astrapaeus* features numerous bifurcate setae that do not form a comb structure (Fig. 16I). Acylophorini displays a protibial comb formed by bifurcate setae. Of the taxa with the running protibiae, Erichsonini, Quediini, *Quedius antipodum*, *Algon*, *Xanthopygus*, and *Staphylinus* all exhibit the protibial comb with bifurcate setae. In *Ocypus*, the character varies, with some species exhibiting bifurcate setae forming combs while others not (Kasule 1970; Boháč 1982). *Eucibdelus* lacks the comb but features small spines scattered on the anterior aspect of the protibia (Fig. 16D). Bifurcate setae are absent in all Philonthina, but in some larger species, combs composed of simple setae are present on the protibia, as observed in *P. spinipes* (for other cases, see Kasule 1970, Kranebitter and Schatz 2002). In our study, *P. spinipes* and the similarly-sized *Algon sphaericollis* were observed using their protibia to comb their mouthparts, suggesting that the comb structures present only in L_2 and L_3 larvae may have a cleaning function. comb of bifurcate setae is also present in *Arrowinus* with the burrowing protibia, but is absent from other Staphylininae with the burrowing protibial type such as *Creophilus* and the *Platydracus* group (Fig. 16E). The diverse set of larval leg phenotypes, paralleling the phenotypes of the complete bodies, indicate a frequent recurrence of plesiomorphic traits and morphological parallelisms during the evolutionary. These convergent and reversal characters may lead to a misleading taxonomic conclusions.

The configuration of paratergites and parasternites on abdominal segment I introduces another layer of diversity among Staphylininae larval features, presenting at least four distinct phenotypes, barring atrophy as seen in species of *Acylophorus* and *Atanygnathus*. The predominant phenotype resembles the typical structure of paratergites and parasternites found in other abdominal segments but the sclerites are slightly reduced and have fewer setae, observed across various tribes such as *Antimerus punctipennis*, *Quedius brevicornis*, *Ocypus fulvipennis*, *Staphylinus erythropterus*, and *Eucibdelus* (Fig. 16J). However, several deviations from this common type exist. For instance, in *Saniderus* and *Arrowinus*, while paratergites maintain their usual form, parasternites are reduced to tiny fragments, accompanied by an additional

lateral sclerite posteriorly (Fig. 16K). A degree of fusion between these fragmented sclerites determines other observed phenotypes, with examples like *Algon sphaericollis*, *Xanthopygus cognatus*, *Astrapaeus ulmi*, *Quedius antipodum* and all species of Philonthina, all fragmented sclerites merge to form an U-shaped lateral sclerite (Fig. 16M), while in certain species of *Platydracus*, including *P. tomentosus*, *P. marmorellus*, and *P. pseudopaganus pseudopatricius*, each paratergite fuses with an additional lateral sclerite, displaying a propensity to bend towards the parasternite (Fig. 16L). Recombination of sclerites is evident at thoracic segments, as seen in *Algon sphaeri-*

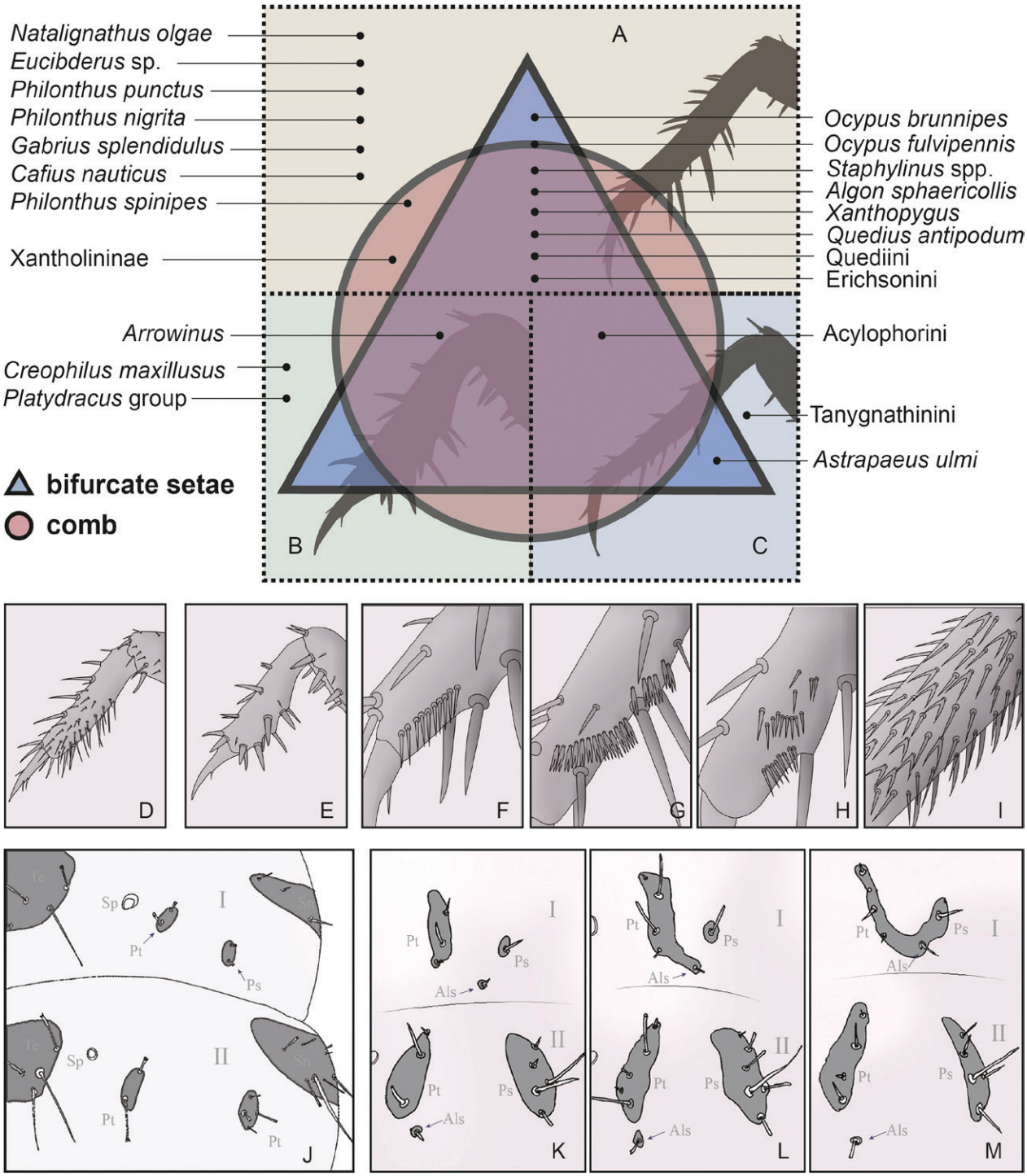

Figure 16. Non-homologous features of Staphylininae. **A**–**I** Mosaic evolution of comb, bifurcate setae on 3 types of protibia. **A** Running type; **B** Burrowing type; **C** Slimmer running type; **J**–**M** The variability of the paratergites and the parasternites of abdominal segment I of Staphylininae. Illustrations indicating characteristic types are represented by the following species: **D**, **J** *Eucibdelus* sp.; **E**, **L** *Platydracus pseudopaganus pseudopatricius*; **F** *Hypnogyra angularis* (after Pietrykowska-Tudruj and Staniec 2006). **G**, **M** *Algon sphaericollis*; **H** *Philonthus spinipes*; **I** *Astrapaeus ulmi* (after Pietrykowska-Tudruj et al. 2014); **K** *Saniderus* sp. — Abbreviations: I, II, abdominal segments; Sp, spiracle; Pt, paratergite; Ps, patasternite; Als, additional lateral sclerite.

collis, where fusion of additional ventral sclerites occurs notably at segment III of thorax (Fig. 6A, B). This diversity underscores the importance of considering parallel evolution when classifying such phenotypes.

3.5. Unusual morphology of examined larvae

Interestingly, our study falls short of providing suitable genus-level diagnoses. *Philonthus* and *Platydracus* appear to be polyphyletic in our trees. We had, nevertheless, observed some genus-specific unusual morphologies:

Eucibdelus, although strongly supported as member of Staphylinina and closely related to *Ocypus*, differs from other Staphylinini by the wide head with a narrow neck, a shorter pygopod, nasale with 11 teeth, protibia without the comb but with small spines scattered on the anterior face and the presence of frayed setae on all three thoracic segments, among others.

Saniderus shares numerous characters with *Platydracus* and is nearly indistinguishable from it, particularly when considering eggs and pupae alone. It can be recognized by the trapezoidal head and the paratergites and parasternites of abdominal segment I not fused.

Philonthus spinipes is characteristic by the whip-like urogomphi, a feature absent in other members of phionthina, but present in unrelated *Ontholestes*, *Abemus*, and *Xanthopygus*. *P. spinipes* differs from other Philonthina by retaining marginal setae on the mala.

Algon sphaericollis differs from other Staphylinini through the notable convergence of paramedian teeth of nasale towards an almost imperceptible median tooth. Additionally, the presence of frayed setae on the meso- and metathorax, but their absence on the prothorax, is a unique trait. *A. sphaericollis* can be discerned from Staphylinina by the U-shaped lateral sclerites on abdominal segment I, when compared to Philonthina, its protibia features a comb with bifurcate setae.

4. Biological traits of the reared Staphylinini species

Habitat. *Algon sphaericollis*, *Platydracus pseudopaganus pseudopatricius* and *Philonthus spinipes* are widely distributed in China, all occurring in Shanghai. They can be found in the urban green spaces as well as in the vegetation of the suburban areas. Both larvae and adults are usually found in moist, loose humus substrate. *Algon sphaericollis* is always attracted to decaying plants but is seldom found under carcasses and dung, where adults and larvae of the other two species can be observed. Decaying bamboo shoots also attract *Platydracus* and *Saniderus*.

Predation. The adults of all five genera prey on most insects of the right size that they come across. In comparison to the larvae of *Saniderus* (Fig. 17C), *Platydracus* and *Philonthus*, larvae of *Algon* are more selective: by offering potential food sources scattered throughout their habitat for larval rearing, we observed that the larvae may feed on ants and Geophilomorpha centipedes (Fig. 17A, B). Nevertheless, they show high mortality and stagnation of the development on the ant-only diet under laboratory conditions. In contrast, they pupated successfully when *Blatta lateralis* was offered as well. *Algon sphaericollis* and *Philonthus spinipes* larvae both have the same type of protibiae (the running type) and frequently roam the humus in search of food. Once encountering the prey, they use knife-like mandibles and saw-like nasale to cut their prey in a scissor-like manner. Notably, the whip-like urogomphi gives *P. spinipes* sharper senses and quick reflexes (Fig. 12A–C) to suit its aggressive hunting style. In contrast, larvae with burrowing-type protibiae (*Platydracus* and *Saniderus*) excavate burrows and ambush for prey. The protibiae of *Eucibdelus* falls between running and burrowing types, but the larva is also a burrow-dweller. Compared to the *Platydracus* group, it displays limited mobility and engages in more passive hunting, waiting for the prey to contact its opening mandibles.

Reproduction. Mating behavior in the laboratory was observed at temperatures around 22°C in all species. When a male and a female were placed together, the male sensed the female and promptly secured her with inflated protarsi. He extended his genitalia and folded forward to initiate mating with the female (Fig. 18A–F). Mating durations varied among species, with *A. sphaericollis* lasting approximately 10 seconds, while species of *Platydracus* and *Saniderus* exhibited mating durations of around 15 seconds. *Eucibdelus* had notably longer mating, lasting approximately half an hour. After a single mating, the female typically lays 1 to 3 eggs every day. The egg-laying period continues until the female's death.

Development. Of the seven species studied here, the complete development was only recorded for *Algon sphaericollis* and *Saniderus* sp. A total of 7 eggs of *A. sphaericollis* successfully hatched in the laboratory, of which 3 successfully developed into adults. The average time from hatching to the emergence of an adult was 39 days. The egg incubation period varied from 4 to 12 days (mean 8.5 days), depending on the size of the egg and the incubation temperature and humidity. The L_1 larvae developed for 1 to 4 days (mean 2.5 days), the L_2 larvae for 3 to 6 days (mean 5 days), and the L_3 developed for 7 to 22 days, (mean 14 days), the prepupa stage lasts for 2 days, and the pupa period is 7 days. The development of *A. sphaericollis* is shown in Fig. 19B.

A total of 26 eggs from *Saniderus* sp. successfully hatched in the laboratory, of which 6 were kept to develop to adults. The average time from hatching to the emergence of an adult was 39 days. The egg incubation period varied from 4 to 7 days (mean 5.1 days). The L_1 larvae developed for 3 to 5 days (mean 4.3 days), the L_2 larvae

for 5 to 7 days (mean 5.5 days), and the L_3 developed for 7 to 22 days, (mean 14 days). the prepupa stage lasts for 2 to 3 days (mean 2.6 days), and the pupa period is 7 to 9 days (mean 7.6 days).

A total of 10 eggs from *Eucibdelus* sp. successfully hatched in the laboratory. The egg incubation period varied from 12 to 15 days (mean 14.6 days). The slow larval development can be attributed to passive predation.

Larvae of each genus pupate in different ways. Mature *A. sphaericollis* larvae burrow into the humus substrate and rearrange the surrounding material to create a simple cavity (Fig. 17D). In contrast, mature *Philonthus spinipes* larvae chew up the surrounding material to construct a well-defined chamber (Fig. 17G). *Platydracus* and *Saniderus* larvae form particularly robust cocoons (Fig. 17E, F). Adult emergence typically occurs in the morning. Newly emerged adults often consume their exuviae. Ventral head, epipleura, prosternum, procoxae, meso- and meta-ventrite take additional time to complete sclerotization after eclosion (Fig. 18G, H).

Figure 17. Living habitus and habitats of larval Staphylinini. **A**–**C** larvae feeding; **D**–**G** prepupating; **A**, **B**, **D** *Algon sphaericollis*; **E** *Platydracus pseudopaganus pseudopatricius*; **C**, **F** *Saniderus* sp.; **G** *Philonthus spinipes*.

Life cycle of *Algon sphaericollis* in Shanghai. Between late October 2020 and early October 2021, a total of 21 adults of *Algon sphaericollis* (7 males and 14 females) and 24 larvae were collected in the field. Adults were observed every month, with a peak in April, while larvae were present from April to June and again from August to October, with the highest larval population occurring in May and June.

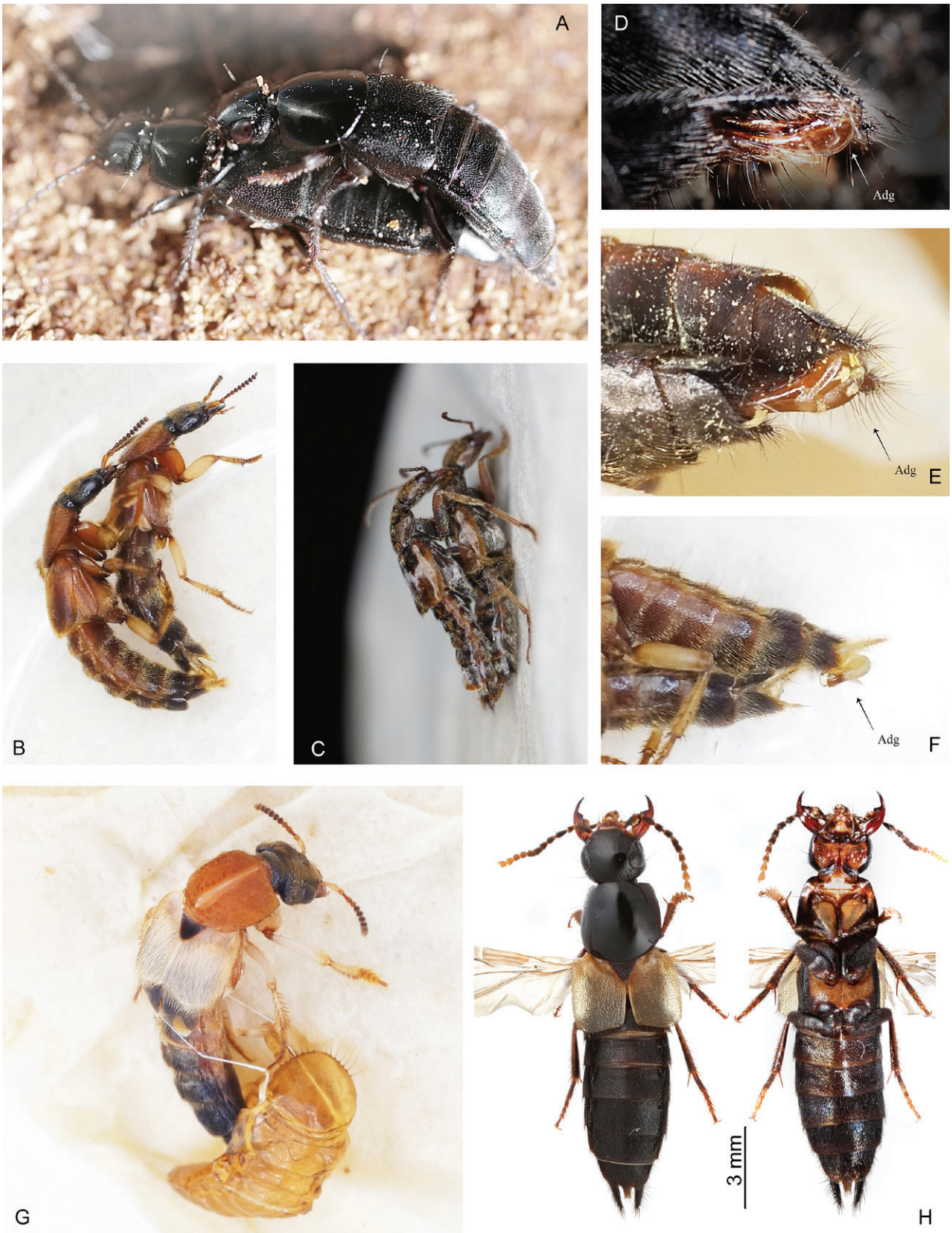

Figure 18. Mating and eclosion of Staphylinini. **A**–**F** Mating, male up in all cases; **G**, **H** newly emerged adult. **A**, **D**, **H** *Algon sphaericollis*; **B**, **F**, **G** *Saniderus* sp., **C**, **E** *Eucibdelus* sp. — Abbreviation: Adg, aedeagus.

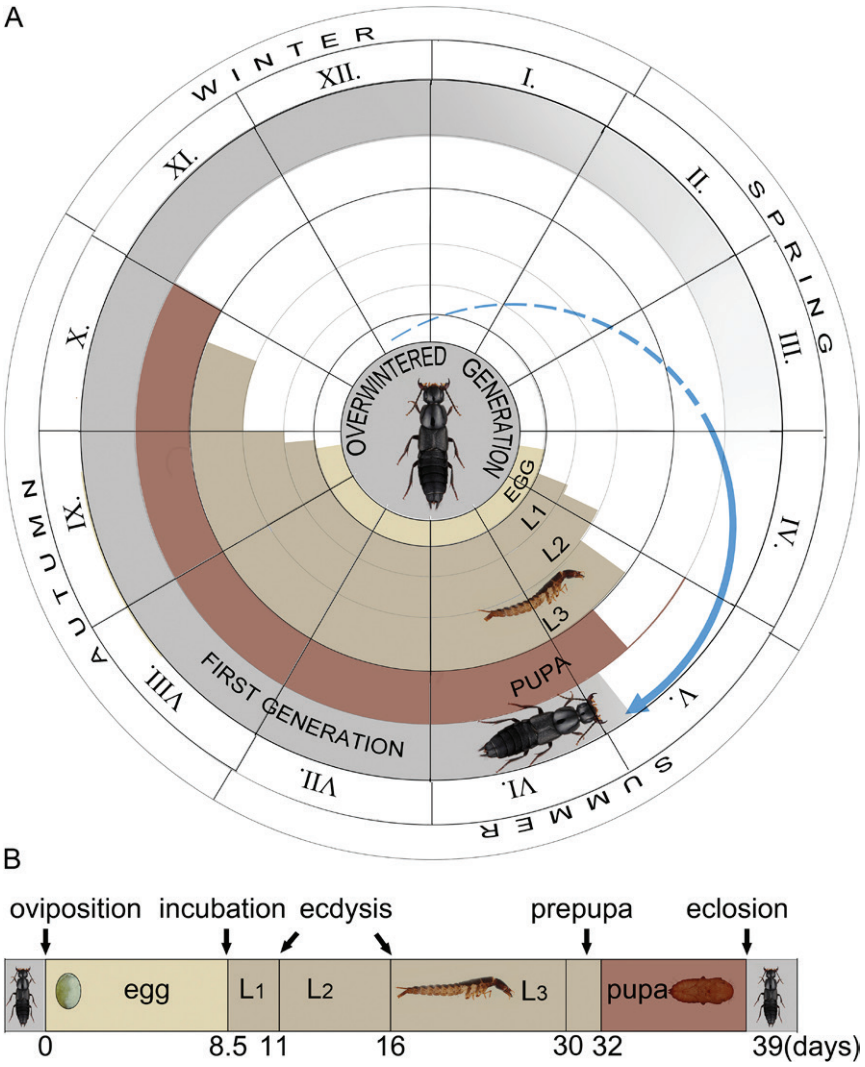

Figure 19. Life cycle of *Algon sphaericollis*. **A** occurrence time of each stage (I.–XII., months, L_1, L_2 and L_3, larval instars); **B** development duration of each stage in the laboratory.

Under laboratory conditions, overwintered adults began laying eggs in mid-April, and continued laying eggs until their deaths in October. A life cycle of *A. sphaericollis* in Shanghai (Fig. 19A) was constructed based on simultaneous observations in the field and the laboratory. We have no evidence of the adults of the new generation would produce offspring in the same year. A similar reproductive strategy has been reported in *Staphylinus* (Boháč 1982) and *Hesperus* (Staniec 2004), although the duration of oviposition in those cases was shorter. The life cycle recorded here applies to the population in Shanghai but may not reflect more northern populations.

5. Conclusions

Detailed morphological data about eggs, larvae, and pupae are valuable to unveil the phylogenetic relationships within the Staphylininae. In many species, the data on immature stages allow to resolve their phylogenetic position with high confidence. In other cases, morphology of preimaginal stages is not enough: resolving the position of some tribes, and the relationships among subtribes and genera, remains challenging. Yet, we firmly believe that data about immature stages holds potential for advancing our understanding of phylogenetic relationships, despite its current limitations due to incomplete knowledge and underexplored morphology. Some character set, like chaetotaxy, are still underutilized, although its utility cannot be overstated (Solodovnikov, 2005). A more extensive set of taxonomic data and detailed morphological studies are required to better understand the diverse immature stages of Staphylininae from the phylogenetic perspective.

6. Acknowledgements

We are grateful to Qing-hao Zhao, who provided living specimens of *Platydracus marmorellus*, *Saniderus* sp. and *Philonthus spinipes* to us for breeding in the laboratory. Thanks to Mei-hua Xia for photographing the eggs of *Saniderus* sp. and *Philonthus spinipes*. Thanks to Wen-xuan Zhang for photographing the habitus of *Eucibdelus* sp. Thanks to Jia-yao Hu (Shanghai Normal University, China) for collecting the living imago of *Algon sphaericollis* in Shanghai and providing valuable advice on larval breeding of *Eucibdelus*. We express our sincere gratitude to Dr. Harald Schillhammer (Austria) for improving the manuscript.

7. References

Ashe JS, Watrous LE (1984) Larval chaetotaxy of Aleocharinae (Staphylinidae) based on a description of *Atheta coriaria* Kraatz. The Coleopterists' Bulletin 38(2): 165–179.

Boháč J (1982) The larval characters of Czechoslovak species of the genera *Abemus*, *Staphylinus* and *Ocypus*. Studie CSAV, Praha, 96 pp.

Brunke AJ, Solodovnikov A (2013) *Alesiella* gen. n. and a newly discovered relict lineage of Staphylinini (Coleoptera: Staphylinidae). Systematic Entomology 38(4): 689–707. https://doi.org/10.1111/syen.12021

Brunke AJ, Smetana A (2019) A new genus of Staphylinina and a review of major lineages (Staphylinidae: Staphylininae: Staphylinini). Systematics and Biodiversity 17(8): 745–758. https://doi.org/10.1080/14772000.2019.1691082

Brunke AJ, Chatzimanolis S, Schillhammer H, Solodovnikov A (2016) Early evolution of the hyperdiverse rove beetle tribe Staphylinini (Coleoptera: Staphylinidae: Staphylininae) and a revision of its higher classification. Cladistics 32(4): 427–451. https://doi.org/10.1111/cla.12139

Brunke AJ, Schillhammer H, Chatzimanolis S (2017) The first fossil rove beetle from the middle Eocene Kishenehn Formation (North America) provides evidence for ancient Eocene relicts within the hyperdiverse Staphylinini (Coleoptera: Staphylinidae: Staphylininae). Journal of Systematic Palaeontology 15(12): 1015–1025. https://doi.org/10.1080/14772019.2016.1266402

Cai YJ, Tang L (2022) Descriptions of the developmental stages of *Cafius nauticus* (Fairmaire) (Coleoptera: Staphylinidae: Staphylininae), with comments on its biology. Zootaxa 5182(5): 429–447. https://doi.org/10.11646/zootaxa.5182.5.2

Chatzimanolis S (2014) Phylogeny of xanthopygine rove beetles (Coleoptera) based on six molecular loci. Systematic Entomology 39(1): 141–149. https://doi.org/10.1111/syen.12040

Chatzimanolis S, Cohen IM, Schomann A, Solodovnikov A (2010) Molecular phylogeny of the mega-diverse rove beetle tribe Staphylinini (Insecta, Coleoptera, Staphylinidae). Zoologica Scripta 39(5): 436–449. https://doi.org/10.1111/j.1463-6409.2010.00438.x

Chatzimanolis S, Brunke AJ (2019) A phylogeny of Xanthopygina (Insecta, Coleoptera) reveals major lineages and the origin of myrmecophily. Zoologica Scripta (1). https://doi.org/10.1111/zsc.12358

Chani-Posse MR, Brunke AJ, Chatzimanolis S, Schillhammer H, Solodovnikov A (2018) Phylogeny of the hyper-diverse rove beetle subtribe Philonthina with implications for classification of the tribe Staphylinini (Coleoptera: Staphylinidae). Cladistics 34(1): 1–40. https://doi.org/10.1111/cla.12188

Dajoz R, Caussanel C (1968) Morphologie et biologie d'un coléoptère prédateur: *Creophilus maxillosus* (L.) (Staphylinidae). Cahiers des Naturalistes, Bulletin des Naturalistes Parisiens 24: 65–102.

Goloboff PA, Farris JS, Nixon K (2008) TNT, a free program for phylogenetic analysis. Cladistics 24: 774–786. https://doi.org/10.1111/j.1096-0031.2008.00217.x

Hinton HE (1981) Biology of Insects Eggs. Pergamon Press, Oxford.

Jeon MJ, Ahn KJ (2005) First larval descriptions for *Cafius Curtis* (Coleoptera: Staphylinidae: Staphylininae) in Korea. Journal of the Kansas Entomological Society 78(3): 261–271.

Kasule FK (1970) The larvae of Paederinae and Staphylininae (Coleoptera: Staphylininae) with keys to the known British genera. Transactions of the Royal Entomological Society of London 122: 49–80.

Kranebitter P, Schatz I (2002) The larval instars of *Philonthus aerosus* Kiesenwetter (subgenus *Kenonthus* Coiffait) from the Central Alps (Tyrol, Austria) with a comparison of the known species of the genus (Coleoptera, Staphylinidae). Entomologische Blätter fur Biologie und Systematik der Käfer 98(1): 61–64.

Lesage L (1984) The larva of *Anaquedius vernix* (Coleoptera: Staphylinidae). The Canadian Entomologist 116(2): 189–196.

Li C, Tang L (2023) New species and records of Algonina Schillhammer and Brunke, 2018, mainly from China. Zootaxa 5256(5): 457–482. https://doi.org/10.11646/zootaxa.5256.5.3

Pietrykowska-Truduj E, Staniec B (2006a) Description of the egg and larva of *Philonthus punctus* (Gravenhorst, 1802) (Coleoptera, Staphylinidae, Staphylininae). Deutsche Entomologische Zeitschrift 53(2): 179–192. https://doi.org/10.1002/mmnd.200600015

Pietrykowska-Truduj E, Staniec B (2006b) The pupae of *Erichsonius cinerascens* Gravenhorst, 1802 and *Heterothops niger* Kraatz, 1868 (Coleoptera: Staphylinidae). Genus 17: 335–342.

Pietrykowska-Tudruj E, Staniec B (2006c) Morphology of the developmental stages of *Hypnogyra angularis* (Ganglbauer, 1895) (Coleoptera, Staphylinidae, Staphylininae). Deutsche Entomologische Zeitschrift 53(1): 70–85. https://doi.org/10.1002/mmnd.200600007

Pietrykowska-Tudruj E, Staniec B (2012) Comparative larval morphology of *Platydracus* and *Staphylinus* (Staphylinidae: Staphylinini: Staphylinina) with notes on their biology and redescription of the pupa of *Staphylinus*. Zootaxa 3580(1): 24–42. https://doi.org/10.11646/zootaxa.3580.1.2

Pietrykowska-Tudruj E, Staniec B, Solodovnikov A (2012) Discovery of the *Quedius antipodum* Sharp larva from New Zealand: phylogenetic test of larval morphology for Staphylinini at the intratribal level (Coleoptera: Staphylinidae). Systematic Entomology 37(2): 360–378. https://doi.org/10.1111/j.1365-3113.2011.00612.x

Pietrykowska-Tudruj E, Czepiel-Mil K, Staniec B (2014) Larval morphology of selected *Quedius* Stephens, 1829 (Coleoptera: Staphylinidae: Staphylinini) with comments on their subgeneric affiliation. Zootaxa 3827(4): 493–516. https://doi.org/10.11646/zootaxa.3827.4.4

Pietrykowska-Tudruj E, Staniec B, Wojas T, Solodovnikov A (2014) Immature stages and phylogenetic importance of *Astrapaeus*, a rove beetle genus of puzzling systematic position (Coleoptera, Staphylinidae, Staphylinini). Contributions to Zoology 83(1): 41–65. https://doi.org/10.1163/18759866-08301002

Pietrykowska-Tudruj E, Staniec B, Wagner GK, Zagaja M (2019) Re-descriptions of mature larvae of two predatory species of *Nudobius* and *Gabrius* associated with bark beetle galleries (Coleoptera: Staphylinidae). Zootaxa 4674(5): 581–599. https://doi.org/10.11646/zootaxa.4674.5.7

Pototskaya VA (1967) Classification key of the larvae of Staphylinidae in the European part of the USSR. Nauka, Moscow, 120pp. (In Russian).

Quezada JR, Amaya CA, Herman Jr LH (1969) *Xanthopygus cognatus* Sharp (Coleoptera: Staphylinidae), an enemy of the coconut weevil, *Rhynchophorus palmarum* L. (Coleoptera: Curculionidae) in El Salvador. Journal of the New York Entomological Society: 264–269.

Rougemont GD (2015) Three new species of *Saniderus* Fauvel, 1895 (Coleoptera: Staphylinidae: Staphylininae) Entomofauna 36: 477–492.

Shaw JJ, Ya D, Solodovnikov A (2020) Molecular phylogeny illuminates Amblyopinini (Coleoptera: Staphylinidae) rove beetles as a target for systematic and evolutionary research. Systematic Entomology 45(2): 430–446. https://doi.org/10.1111/syen.12405

Schillhammer H (2006) Revision of the genus *Algon* Sharp (Coleoptera: Staphylinidae: Staphylininae). Koleopterologische Rundschau 76: 135–218.

Schmidt DA (1994a) Notes on the biology and a description of the egg, third instar larva and pupa of *Platydracus tomentosus* (Gravenhorst) (Coleoptera: Staphylinidae). The Coleopterists' Bulletin 48(4): 310–318.

Schmidt DA (1994b) Notes on the biology and a description of the egg, third instar larva and pupa of *Neobisnius sobrinus* (Coleoptera: Staphylinidae). Transactions of the Nebraska Academy of Sciences 21: 55–61.

Schmidt DA (1996) Description of the immatures of *Erichsonius alumnus* Frank and *E. pusio* (Horn) (Coleoptera: Staphylinidae). The Coleopterists' Bulletin 50(3): 205–215.

Solodovnikov A (2005) *Natalignathus*, gen. nov. and larvae of *Atanygnathus*: a missing phylogenetic link between subtribes Quediina and Tanygnathinina (Coleoptera: Staphylinidae: Staphylininae: Staphylinini). Invertebrate Systematics 19(1): 75–98. https://doi.org/10.1071/is04031

Solodovnikov A, Newton AF (2005) Phylogenetic placement of Arrowinini trib.n. within the subfamily Staphylininae (Coleoptera: Staphylinidae), with revision of the relict South African genus *Arrowinus* and description of its larva. Systematic Entomology 30(3): 398–441. https://doi.org/10.1111/j.1365-3113.2004.00283.x

Solodovnikov A, Schomann A (2009) Revised systematics and biogeography of 'Quediina' of sub-Saharan Africa: new phylogenetic insights into the rove beetle tribe Staphylinini (Coleoptera: Staphylinidae). Systematic Entomology 34(3): 443–466. https://doi.org/10.1111/j.1365-3113.2008.00468.x

Solodovnikov A, Newton AF (2010) Revision of the rove beetle genus *Antimerus* (Coleoptera, Staphylinidae, Staphylininae), a puzzling endemic Australian lineage of the tribe Staphylinini. Zookeys 67: 21–63. https://doi.org/10.3897/zookeys.67.704

Solodovnikov A, Yue Y, Tarasov S, Ren D (2013) Extinct and extant rove beetles meet in the matrix: Early Cretaceous fossils shed light on the evolution of a hyperdiverse insect lineage (Coleoptera: Staphylinidae: Staphylininae). Cladistics 29(4): 360–403. https://doi.org/10.1111/j.1096-0031.2012.00433.x

Staniec B (1999) A description of the pupae of *Quedius fumatus* (Stephens), *Quedius humaralis* Stephens, *Quedius mesomelinus* (Marsham) and *Quedius fuliginosus* (Gravenhorst) (Coleoptera: Staphylinidae: Staphylininae). Genus 10: 47–57.

Staniec B (2003) Morphology of the mature larva and pupa of *Quedius brevicornis* (Thomson, 1860) (Coleoptera: Staphylinidae). Annales Zoologici 53(4): 673–680.

Staniec B (2004) Description of the developmental stages of *Hesperus rufipennis* (Gravenhorst, 1802) (Coleoptera: Staphylinidae), with comments on its biology. Annales Zoologici 53(3): 287–500.

Staniec B (2005a) A description of the developmental stages of *Acylophorus wagenschieberi* Kiesenwetter, 1850 (Coleoptera, Staphylinidae), with comments on its biology, egg parasite and distribution in Poland. Deutsche Entomologische Zeitschrift 52(1): 97–113. https://doi.org/10.1002/mmnd.200210003

Staniec B (2005b) Description of the developmental stages of *Atanygnathus terminalis* (Erichson, 1839) (Coleoptera, Staphylinidae, Staphylininae), with comments on its biology. Deutsche Entomologische Zeitschrift 52(2): 173–190. https://doi.org/10.1002/mmnd.200410011

Staniec B, Pietrykowska-Tudruj E (2005) The pupae of *Tasgius* (= *Ocypus* sensu lato) *melanarius* (Herr, 1839) and *Quedius cruentus* (Olivier, 1795) (Coleoptera: Staphylinidae). Genus 16(1): 19–28.

Staniec B, Pietrykowska-Tudruj E (2007) Comparative morphology of the eggs of sixteen Central European species of Staphylininae (Coleoptera, Staphylinidae). Deutsche Entomologische Zeitschrift 54(2): 235–252. https://doi.org/10.1002/mmnd.200700021

Staniec B, Pietrykowska-Tudruj E (2008) Morphology of the immature stages and notes on biology of *Philonthus nigrita* (Gravenhorst, 1806) (Coleoptera, Staphylinidae) a stenotopic species inhabiting *Sphagnum* peatbogs. Deutsche Entomologische Zeitschrift 55(1): 167–183. https://doi.org/10.1002/mmnd.200800015

Staniec B, Pietrykowska-Tudruj E (2010) The first description of the mature larva of *Bisnius nitidulus* (Gravenhorst, 1802) (Coleoptera: Staphylinidae). Genus 21(2): 205–217.

Staniec B, Pietrykowska-Tudruj E (2019) Pupae of the mega-diverse rove beetle tribe Staphylinini (Coleoptera, Staphylinidae): their traits and systematic significance. Zookeys 877: 133–159. https://doi.org/10.3897/zookeys.877.35715

Staniec B, Pilipczuk J, Pietrykowska-Tudruj E (2009) Morphology of immature stages and notes on biology of *Ocypus fulvipennis* Erichson, 1840 (Coleoptera: Staphylinidae). Annales Zoologici 59(1): 47–66. https://doi.org/10.3161/000345409X432583

Tihelka E, Thayer MK, Newton AF, Cai C (2020) New Data, Old Story: Molecular data illuminate the tribal relationships among rove beetles of the subfamily Staphylininae (Coleoptera: Staphylinidae). Insects 11(3): 164. https://doi.org/10.3390/insects11030164

Voris R (1939) The immature stages of the genera *Ontholestes*, *Creophilus* and *Staphylinus* Staphylinidae (Coleoptera). Annals of the Entomological Society of America 32(2): 288–303.

Żyła D, Solodovnikov A (2019) Multilocus phylogeny defines a new classification of Staphylininae (Coleoptera, Staphylinidae), a rove beetle group with high lineage diversity. Systematic Entomology 45(1): 114–127. https://doi.org/10.1111/syen.12382

Zhao QH, Solodovnikov A (2023) Immature stages of the remarkable and rare West Palaearctic rove beetle *Emus hirtus* (Coleoptera: Staphylinidae: Staphylinini) in the phylogenetic context of the subtribe Staphylinina. European Journal of Entomology 120: 105–114. https://doi.org/10.14411/eje.2023.013

Supplementary Material 1

File S1

Authors: Li C, Tang L (2024)
Data type: pdf
Explanation notes: Data matrix of 71 characters of immature stages scored for 40 species of 30 genera.

Link: https://doi.org/10.3897/vz.74.e106391.suppl1